$\begin{array}{c} {\rm Two\text{-}Phase\ Flows} \\ {\rm in} \\ {\rm Gas\text{-}Evolving\ Electrochemical\ Applications} \end{array}$

by

Ruben Wetind

October 2001
Royal Institute of Technology
Department of Mechanics
FaxénLaboratoriet
SE-100 44 Stockholm, Sweden

Typsatt i $\mathcal{A}_{\mathcal{M}}\mathcal{S}$ - $\mathbb{A}_{T_{E}}X$.

Akademisk avhandling som med tillstånd av Kungliga Tekniska Högskolan i Stockholm framlägges till offentlig granskning för avläggande av teknologie doktorsexamen fredagen den 12:e oktober 2001, kl. 13.15 i Kollegiesalen, Administrationsbyggnaden, Kungliga Tekniska Högskolan, Valhallavägen 79, Stockholm.

©Ruben Wetind

Tryck: Universitetsservice US AB, Stockholm 2001

 $\begin{tabular}{ll} To \ my \ Mother \\ and \\ the \ Memory \ of \ my \ Father \\ \end{tabular}$

Two-phase flows in gas-evolving electrochemical applications

Ruben Wetind

FaxénLaboratoriet, Kungliga Tekniska Högskolan, SE-100 44 Stockholm, Sweden October, 2001

Abstract

This thesis deals with two-phase flows in gas-evolving electrochemical applications. Many important electrochemical processes involves evolution of gas. Some examples are the chlorate process, the chlor-alkali process, aluminium electrolysis in chryolite baths, zinc electrowinning as well as the pickling of steel. The presence of gas can affect the processes in different ways. In the idealised case the rising gas bubbles induce an internal circulation in the reactor which continuously carries fresh electrolyte to the electrodes. On contrary, the worst case involves a dramatic conductivity deterioration in the gas/electrolyte as well as a reduction of active electrode area due to partwise coverage of gas. As a matter of fact, it appears that a small modification might be enough to turn a well working process into a hardly working, or the opposite way. The aim of this thesis is to investigate some of the factors which may affect the efficiency of a gas-evolving electrochemical system.

The major part of this thesis involves numerical simulations using two different hydrodynamical two-phase models. The first, a two-fluid model with inclusion of turbulence for the liquid phase, is used for a full scale study of the buoyancy induced circulation in a conceptual gas-evolving chlorate reactor. Design matters are discussed and some explicit recommendations, based on results from this study, are presented. An analytical relation for prediction of the electrolyte circulation rate is further suggested. Secondly, a mixture model is used for studies of both forced and free convection of the bubbly flow between two electrodes. Necessary closure laws for the relative velocity between the phases are based on empirical relations for particle suspensions. The mixture model is further extended to include mass-transport of ionic species with the aim to predict non-uniform current density along the electrodes. Parameter studies show that the bubble size has a major influence on both distribution and magnitude of the buoyancy induced velocity.

Complementary experimental data from bubbly flow in a vertical pipe is presented together with tests of new experimental equipment and measuring techniques. The micro-bubble suspension is investigated by mean of image analysis and the use of a new fibre optics velocimeter. Typical results include the distributions of void fraction and velocity. A special device for electrochemical production of hydrogen bubbles is constructed and tested. The measured size distribution of the bubbles shows that the appliance can be used to generate bubbles of size $100 \pm 40 \ \mu m$

Descriptors: two-phase flow, electrochemical, reactor, chlorate, micro-bubbles, two-fluid model, numerical modelling, mixture model, drift-flux model, gas-evolving, electrolysis, current distribution, dispersion, image analysis, laser-sheet, fibre optics.

List of papers

- Paper 1. Wedin R., Dahlkild A. A numerical and analytical hydrodynamic two-phase study of an industrial gas-lift chlorate reactor. *Computational technologies for fluid/thermal/structural/chemical systems with industrial applications 1*, ASME (1999), PVP-Vol. 397-1, 125-136.
- **Paper 2**. Wetind R., Dahlkild A. A hydrodynamical model for the dispersal of small bubbles under developing channel flow. *Submitted to J. Appl. Electrochem.*, (2001)
- Paper 3. Wedin R., Davoust L., Cartellier A., Dahlkild A. A mono-modal fiber-optics velocimeter for electrochemically generated bubbles. *Proceedings of Tenth International Symposium on Applications of Laser Techniques to Fluid Dynamics*, Lisbon, (2000)
- **Paper 4**. Wedin R., Davoust L., Cartellier A., Byrne P. Experiments and Modeling on Electrochemically generated bubbly flows. Presented at 4th ICMF New Orleans 2001. To appear in special issue of Elsevier journal- ETFS.
- Paper 5. Wedin R., Dahlkild A. On the transport of small bubbles under developing channel flow in a buoyant gas-evolving electrochemical cell. Presented at CRE VIII 24-29 June (2001), Barga, Italy *To appear in special issue of Ind. Eng. Chem. Res.* 2001
- **Paper 6**. Wetind R. Modelling the mass transport and two-phase flow in a gasevolving electrochemical cell. *Submitted to J. Electrochem. Soc.* (2001)

NOTE:

The author has during the course of work altered the family name from Wedin to Wetind.

Articles by the author not included in the thesis.:

Bark F.H., Kharkats Y.I., Wedin R. Joule heating in electrochemical cells. *Proceedings of Third KSME-JSME Thermal Engineering Conference*, Vol. 2, pp. 9-17. (1996), Kyongju, Korea.

Kharkats Y.I., Bark F.H., Wedin R. On the theroretical aspects of thermal effects in electrochemical cells. *J. Electroanal. Chem* Vol. 450, pp. 37-45. (1998).

The thesis is re-set in the present latex format. Minor layout revisions are made on the articles which are previously published. Section 2.7 in paper 1 is slightly extended, here providing the derivation of the analytical relation.

Division of work between authors:

All coding and numerical simulations within the frame of this thesis are performed by Ruben Wetind. He also analysed the results as well as wrote and illustrated the articles. Anders Dahlkild contributed with suggestions of mathematical models, revision of the written text and many comments on the analyse of the results.

Wetind and Philip Byrne designed the experimental device EBBA, which then were built under the control of Byrne. The measurments reported in paper 3 and 4 are performed by Wetind with suggestions on the experimental procedure and equipment by Laurent Davoust and Alain Cartellier. They also contributed with suggestions on the analysis of data as well as a revision of the text. The vertical pipe which was used for the experiments in paper 4 is previously designed and constructed by the group of Cartellier.



Contents

List of papers	vi
Chapter 1. Introduction 1. Historical Background 2. Gas-Evolving Electrochemical Cells	$\begin{array}{c} 1 \\ 1 \\ 7 \end{array}$
Chapter 2. Basic Hydrodynamical Concepts 1. Single-Phase Flow 2. Two-Phase Flow 3. Some Dimensionless Parameters	10 10 12 20
Chapter 3. Basic Electrochemical Concepts 1. Reaction Kinetics at Electrodes 2. Mass Transport in the Electrolyte	22 22 28
Chapter 4. A Short Presentation of the Work 1. Computational Work 2. Experimental Work 3. The Papers	30 30 32 35
Chapter 5. Outlook 1. Improvements of the Techniques, Tools and Models 2. A New Generation of Electrochemical Reactors	49 49 50
${ m Acknowledgments}$	52
Bibliography	53
Paper 1:	
Paper 2:	
Paper 3:	
Paper 4:	
Paper 5:	
Paper 6:	

Introduction

1. Historical Background

In everyday life, we are used to encounter three states of matter: solid, liquid and gas. Most people can intuitively and quite easily sort a substance into one of the three phases.

It hurts to drop a dense solid on your feet; you can swim in a liquid and fly in a gas

Although liquids and gases are different in many aspects, they share common characteristics in which they clearly differ from solids. They are fluids which deforms continuously under the action of shearing forces for as long as the force is applied. As the fluid is unable to retain any unsupported shape, it flows under its own weight and shapes after any solid objects who are brought into contact with the fluid. Despite the similarities between liquids and gases, they also have many typical characteristics of their own. Liquids are difficult to compress and can most often be considered to be incompressible. A given mass of a liquid occupies a certain volume and if the tank who holds the liquid is larger than this volume the liquid will form a free surface. A given mass of a gas is not connected to any fix volume. The gas can be compressed into a small tank under hard pressure, or conversely expand to fill a larger one. A free surface will not be formed.

Even though a fluid is understood to deform under shearing forces, there is still a large variation between fluids in their behaviour under stress. Most common fluids are known as Newtonian fluids. These fluids are categorised by obeying the following relation for the shear stress

$$\tau = \mu \frac{\partial u}{\partial y}$$

i.e. the shear stress, τ , is proportional to the velocity gradient of the fluid, and μ is a property of the fluid known as the coefficient of viscosity.

On contrary, non-Newtonian fluids alter the viscosity with the rate of the shear or with the elapsed time for which a shearing force is applied. Examples of non-Newtonian fluids are blood, cement, ketchup, quicksand and thixotropic jelly paints.

The field of fluid dynamics has been extensively studied throughout the history. ([49], [40], [2], [1], [21]). From an early age, man has had sufficient empirical knowledge in order to build ships and boats. A starting point for the more questioning search could be when Greece native Archimedes (287-212 B.C.) during a visit at a public bath discovered the elementary principles of buoyancy, and then according to the legend ran naked down the streets shouting 'Eureka, eureka!". During these years, the focus of the research were however laid on pumping techniques and the development of water distribution systems, such as

1

the Roman aqueducts which Sextus Julius Frontinus (40-103 A.D.) wrote about. It could be mentioned that the water-screw invented by Archimedes (figure 1.1) is still used to lift water in parts of the world.

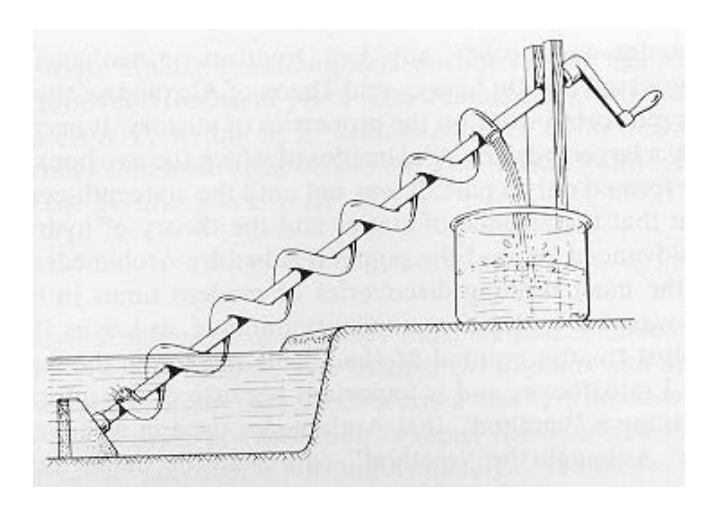


FIGURE 1.1. The Archimedes water-screw.

In these early years it is possible that also the field of electrochemistry was born. Today, at the Bhagdad museum in Iraq, an object is exhibited, claimed to be the first battery. This ancient "battery" origins from the days of Jesus Birth. Together with findings of copper vases covered with a thin layer of silver, many have drawn the conclusion that these old batteries was actually used for plating of objects. Whether this is scientificly proved or not is left for others to decide, but the thought is exiting.

Another starting point for research on the subject of fluid dynamics as we know it today, could be when the multi talented Renaissance-man Leonardo Da Vinci (1452-1519) performed water experiments based upon flow visualisation. Especially under the years 1506-1508 which he spent in Milan, Italy, he observed and sketched many basic flow phenomena. Da Vinci also expressed the elementary principle of continuity, and suggested designs for hydraulic machinery.

A number of additional inputs to the field were given during the succeeding century. An interesting contribution was given by the French physicist Edme Mariotte (1620-1684) who built the first wind-tunnel. Blaise Pascal (1623-1662), a young French mathematical genius, proceeded Evangelista Torricellis (1608-1647) work on atmospheric pressure and explained the principles of the barometer. Pascal also investigated the nature of hydraulic pressure, a matter which was further clarified by Henri de Pitot (1695-1771) who designed a device, today known as the Pitot tube, with which water velocity could be estimated through differential head.

Until now, the science of electrochemics had not been developed with the same speed as the hydrodynamics. Much due to the fact that electricity itself was not controlled. One of the early pioneers, Benjamin Franklin (1706-1790), proved



FIGURE 1.2. Benjamin Franklin with kite during a thunderstorm.

in the latter part of the 18th century that electricity has a positive and a negative charge and invented an advanced electrical machine with leather friction cushion and glass globe. He is however perhaps most known for his risky experiments in which he flew metal-tipped kites during thunderstorms and "captured the fire of heaven", figure 1.2. By experimenting with different metals and shapes he was able to perfect his famous lightning rod conductor. Alessandro Volta (1745-1827), a professor of philosophy at Pavia, contributed much to electrical and electrochemical science. He introduced the theory of electrical current and observed electricity as he separated water into its component parts of hydrogen and oxygen. The year 1800 Volta constructed the "Voltaic pile" (figure 1.3), made of alternating copper and zinc discs, with each pair of metals separated by flannel soaked in weak acid. Electricity could now be electrochemically produced and controlled to flow evenly in a closed circuit. The modern battery was born!

Important contributions to the field of electrochemistry were also given by Michael Faraday(1791-1867). He systematised electrochemical terms, and stated the first and the second Laws of Electrolysis:

- (i) the substance mass generated by an electrolytic reaction is proportional with the amount of electricity passed through the cell, and
- (ii) one equivalent weight of a substance is generated at each electrode during the passage of 96487 coulomb of charge through an electrolytic cell.

For young students of today, the first lesson of their first fluid dynamic course most often includes the Bernouillis equation

$$p + \frac{\rho}{2}u^2 = const$$

which states the fundamental relationship between pressure and velocity along a streamline. Even though the name of the equation aim at Daniel Bernoulli (1700-1782) via his major work Hydrodynamica, it was actually Leonhard Euler (1707-1783) who obtained the necessary understanding to state that the pressure actually was a point property which is variable in the fluid. He derived a differential equation which he then integrated to the form which is commonly known as the Bernouilli equation. In fact, Eulers teacher, Johann Bernoulli (1667-1748), was actually the father of Daniel Bernouilli, and it is clear from the fathers main work Hydraulica that also he had a deeper insight into the matter than Daniel Bernoulli. Perhaps no other scientist worked with the same intensity as Euler did. His total work included 886 books and papers - and 13 children.

Channel flow was carefully investigated by Antoine Chezy (1718-1798), who managed to formulate general relations, so measurement from one channel could be used for prediction of the flow in another.

As mathematical tools, such as the functional analysis, were developed, a number of prominent authors presented solutions on central problems. Joseph-Louis Lagrange (1736-1813) and Pierre-Simon Laplace (1749-1827) produced for example many advanced solutions of inviscid flow problems.

A major contribution was given by Eulers succeeder as director of mathematics at the Berlin Academy of science, Marie Henri Navier (1785-1836), who the year 1821 presented the complete equations of motions for an incompressible fluid as we now them today - the Navier-Stokes equations.

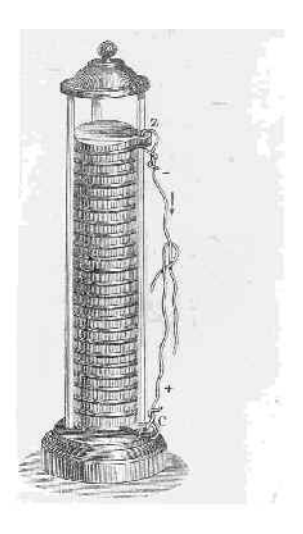


FIGURE 1.3. The Voltaic pile; the first modern battery.

During the 19th century, piece after piece were laid on the fluid dynamic theory as we know it today. The methods to solve these more and more complicated relations were, however, not developed until the second half of the 20th century.

Important steps for the science were further made by Gotthilf Hagen (1797-1884) who studied the transition between laminar and turbulent flow, Jean Poiseuille (1799-1869) who performed meticulous tests on resistance of flow through capillary tubes and Henri Darcy (1803-1858) who carried out extensive tests on

filtration and pipe resistance. The man behind the Froude number, William Froude (1810-1871), developed the conversion of wave and boundary layer resistance from model to prototype scale.

Of great importance for the knowledge of fluid dynamics were the works by the Irish born George Gabriel Stokes (1819-1903). Except that he gave a major contribution with his studies of settling spheres in viscous fluids, he also provided analytically derived relationships on a number of fields ranging from wave mechanics to motion of incompressible fluids. He was actually the first person to visualise the motion of a fluid element as the resolution of the three components: translation, rotation and strain. Stokes placed the equations derived by Navier on a more rigorous basis, and via the perhaps most known equation in fluid dynamics, the Navier-Stokes equation, will his name remain in the history.

Another name frequent encountered in the field is the one by Osborne Reynolds (1842-1916). The perhaps most known non-dimensional number of all in fluid dynamics, the Reynolds number is named after him. He performed experiments in many fields such as cavitation and pipe resistance, and in 1886 he formulated a theory of lubrication.

Another famous dimensionless number is the one called up after the Cambridge professor Lord Rayleigh (or John William Strutt, which was his real name) (1842-1919). He is one of the few scientists working with fluid dynamics who has earned the Nobel Prize (although that was for the discover of the inert gas Argon) . His main contributions to the field included studies of for example bubble collapse, wave motion and the instability of jets.





FIGURE 1.4. (Left) Airplane pioneer Lyman Gilmore with his brother. (Right) The Wright Brothers during their first flight.

Until the beginning of the twentieth century the total knowledge of hydrodynamics had indeed increased considerably since the days of Archimedes. Many fundamental flow phenomena were now described with advanced mathematical relations. New areas of interests became for example the boundary layer theory, instability of flow and the challenging field of turbulence. These new topics were also of increasing importance since the Wright Brothers 1903 in South Carolina conquered the sky with the first airplane. Whether it actually was the hermit Lyman Gilmore who performed the first flight already 1902 in North Carolina could however be discussed; all the same the airplane was invented. The airborn rivals are shown in figure 1.4.

At the same time as the news of the flying planes spread over the world, the professor of mechanics at the University of Hanover, Ludwig Prandtl (1875-1953), conceived the idea of the boundary layer, which adjoins the surface of a

body moving through a fluid. He showed that the flow around an object could be divided into two principal regions. The first consisting of a thin layer near the surface of the body where the frictional effects of the viscous forces plays an important role. The second region which is situated outside this viscous region, where the flow can be considered inviscid. The direct gain of his foundings were that the equations of motions could be simplified in the different regions of the flow field. Prandtl also contributed to the field of turbulence where he introduced the mixing length theory. One of Prandtl's students, Heinrich Blasius (1883-1970), then continued Prandtl's work and derived an analytical solution to the boundary layer equations.

Numerous other persons have given a minor or major input on the subject of fluid dynamics and it is impossible to mention all prominent individuals in just a brief introduction. During the twentieth century the scientific development became enormous. Even if the basic equations were established already in the latter part of the 18th century, proper numerical methods to solve the equations did not appear until the second half of the 20th century.

A tremendous development of computational power has also rendered the possibility to solve complicated coupled differential equations, and new doors have been opened for the establishment of fluid dynamic knowledge, [20]. As a matter of fact, increase in computational speed during the last 30 years has been a factor of ten every five years. The introduction of modern computers renders the possibility to solve complicated coupled differential equations. The prediction of turbulence as well as the subject of this article, two-phase flow, involves most often very large computations, and the possibilities to do new findings in these fields are quite suddenly many. Not only the computational technique has improved under the last century. Hand in hand have also the measuring techniques improved. The existence of fast electronic devices, lasers, sensors, etc. have had a large impact on the field. Actually, a large number of the multi-science researcher from the 17th and the 18th century, mentioned above, also developed much of the optical technique used today in LDV, PDA and PIV measurements.

As pointed out by Walsh [56], the early developments of electrochemistry as a science was self-hindering due to its focus on equilibrium, reversible reaction kinetics. Although early contributions, [7], were made by Tafel (1905), Butler(1924), Volmer & Erdey-Gruz (1930) and the Frumkin group (1930 onwards) it was not until the sixties that the application of techniques based on the interpretation of current versus potential commenced. But still at that period, lack of reliable potentiostatic equipment constrained many studies. Walsh also suggests that the slow start for electrochemical engineering could be explained by a weak profilation of the field for new students. Also the reality that important disciplines of industrial electrochemistry such corrosion, batteries, electroplating etc. have developed somewhat isolated from each other, could be put forward as an answer to the point at issue.

For a large variety of industrial areas computer-simulations has today become an important method to investigate existing processes and in the development of new production techniques. The cost of an engineer with computer and a commercial CFD (Computational Fluid Dynamics) software are in most cases dramatically below the price of a full scale flow experiment. Even if experiments seldom can be totally avoided, a carefully planned set of numerical simulations can point out important aspects and direct the experimental studies to the most

interesting features. Although the use of simulations are more frequent in fluid dynamics than in electrochemistry.

2. Gas-Evolving Electrochemical Cells

The subject of this thesis is devoted to gas-evolving electrochemical cells and reactors. In these processes the the actual gas production is seldom the principal goal, but rather a side-effect. Typical examples are the chlorate process, the chloralkali process, zink electrowinning, electrolytic pickling, aluminium production in chryolite baths etc. Indeed, in a majority of the most important industrial electrochemical processes, gas is evolved.

These industrial reactors often consists of planar electrodes, vertically positioned with constant spaces.

The electrolyte is convected upwards between the electrodes either by some external pump mechanism or by making use of the gas-lift effect, in which the buoyancy induced on the gas bubbles are transferred to the electrolyte via the interfacial drag forces. In the latter case the gas-lift can be used to promote a global circulating flow in the reactor which continuously carries fresh electrolyte to the electrodes. The flow set up locally between the electrodes is then a forced convection, although, as will be demonstrated in this study, effects of buoyancy may not always be neglected there.

Gas evolution can, however, also give unwanted effects such as ohmic fluctuations, irregular current distribution and gas-covered electrode surfaces. This is encountered in the case with electrolytic pickling of steel bands, where the actual electrode surface is horizontal and the negative effects in form of reduced active electrode area is a sincere problem. The interest in such multi-phase flows has increased rapidly during the last few years. By tradition and due to the complicated nature of the problem, much of the research in this area has been experimental.

Reactors with electrolyte circulation driven by the buoyancy of produced gas are generally equivalent to air-lift reactors (ALR). The subject of ALR is due to its diverse applicability important and has frequently been investigated. For an extensive insight in this matter the reader is advised to Chisti (1989) [13]. As environmental concern accelerated in the end of the eighties, a new application for air-lift reactors appeared: the bioreactor, which was used for example in waste-water treatment where a gas flow ensures both oxygen supply and mixing. Different authors have, during the last years, made considerable work to investigate the mechanics of the system and optimise the process in order to receive high mass transfer and efficient mixing at a low consumption of energy. When, for example, Ghirardini et al. [22] measured scale-up effects for an ALR, they found a positive scale effect, suggesting that larger reactors have a higher efficiency. The same year Lindert et al. [36], demonstrated that one of the most important geometric parameters turned out to be the reactor height. As described in paper 1, the equivalent parameter for a chlorate reactor is the chimney height.

Until the 1990th decade most mathematical models of ALR were based on simple 1D assumptions. Cockx et al. [14] were pioneeric and performed numerical 3D-simulations using the CFD-code ASTRID. They provided numerical space-averaged results to obtain closure relations for a simpler analytical 1D-model. Previously the closure relations were achieved by using experimental data. The advantage of the model was a more general technique than global correlations

and less complicated than full 3D-simulations.

One aim of the present work is to set up a simulation model for describing and investigating the major flow patterns in a conceptual electrochemical reactor with vertical electrodes mounted in a stack close to the bottom of a large tank, e.g. a chlorate reactor. Such a model makes possible a convenient testing of the running performance, and can indicate weak points of the reactor design. Typical questions which needs further investigation are for example:

- (i) how the lift velocity can be increased by a scaling of the reactor
- (ii) what should be considered in a re-design of the reactor.

In paper 1 (this thesis) a numerical study of these questions and other are performed, and some suggestions for a good design is presented.

Gas-evolving electrodes and the production and behaviour of especially hydrogen gas in electrochemical processes has been studied by many previous authors. Important contributions are made by Vogt [55]. In his work he demonstrates that the production of gas can be divided in different characteristic steps and regimes at the electrodes. The first, in which the current density is very low and the dissolved gas is removed from the electrode in the direction of liquid bulk by molecular diffusion and usually by superposed liquid convection. The second, with increased current density, where gas bubbles form at predestined nucleation sites at the electrode. The bubble growth is due to supply of dissolved gas from the surrounding electrolyte. A further increase of current density results in a higher super saturation of gas in the electrolyte. Then, with additional sites activated, the bubbles will finally touch each other and cover the whole electrode as a gas film which will incessantly collapse and reform. Contrary to the common view, he also demonstrated that the evolution of gas at an electrode only to a low degree occurred at the electrode. Instead, most of the evolution actually occurred in a zone of super saturated electrolyte close to the electrode. Using two independent methods he derived expressions for the rate of gas evolution at

Regarding the mass transfer at gas-evolving electrodes, this matter has been extensively investigated by Janssen in a number of publications, which are best reviewed in [31]. One of his major result is that mass transfer is strongly promoted by gas evolution.

Coalescence, or the lack of it, are determined by the properties of the gas, the bubbles and the electrolyte [35] and [37]. Systems with coalescence experience effects on mass transfer and electrochemical properties which are not possible to neglect, [31]. Also from an hydrodynamical point of view, this feature must be considered. In the studies included in this work, which mostly concerns hydrogen bubbles, coalescence is estimated not to be of major importance and is therefore not considered. In conditions where the bubbles have a strong surface tension, collisions rather than coalescence can occur between the bubbles. The phenomena of collisions are described in detail by Prince & Blanch [43].

The flow in gas-evolving vertical electrochemical cells are previously studied by a number of authors. A majority of these studies are experimental, and with no special focus on the distribution of the gas bubbles, nor of the velocity in the channels. Indeed, the idea that the flow itself is a somewhat independently developed phenomena has been frequently used. The explanation to put forward is the lack of reliable experiments on flow distribution in gas-evolving cells as well as lack of mathematical modelling connecting the full problem including both two-phase flow and electrochemical reactions. It turns out that although two-phase channel flow (or more common - pipe flow) is a popular area for experimental research, the studies of very small bubbles ($\sim 10-100~\mu m$) is difficult due to a high interfacial area density, prohibiting the use of most common measuring techniques. LDV, PDA etc. are difficult as the mixture can not be penetrated by a laser beam. The problematics of this matter is discussed more extensively in paper 3 and 4 in this thesis. Visualisation fails for the same reason. Optical fibres as a velocimeter are tested recently (thesis paper 3) and could be a promising tool

Some mathematical contribution on this subject is donated by Bankoff [4] who presented the velocity profile in terms of a 2D power law expression. Another work to be mentioned is the presentation of a simplified drift flux model by Zuber & Finlay [58]. Related studies are also performed by Ziegler & Evans [57], Hine [25], Hine & Murakami [26], Wallgren & Bark [53]. Byrne et al. contributed to the subject in their numerical and experimental studies of the chlorate reactor as well as the distribution of gas and velocity in a small electrochemical cell.

The present thesis was prepared parallel with the work by Byrne et al. [9], [10] and [11]. The works are therefore in some matters closely related (specially thesis paper 5 which in its turn are based on paper 2). A step towards a fully coupled electrochemical and hydrodynamical model was taken recently by Dahlkild [18], who used a drift flux two-phase model to describe the distribution of gas and velocity next to an electrode with the evolution of gas described by Tafel laws. Paper 6 in the present thesis is an extension of this work to be valid in a 2D channel with two gas-evolving electrodes.

Basic Hydrodynamical Concepts

1. Single-Phase Flow

The major part of this thesis will discuss phenomena which belong to the field of two-phase flow. Whereas the fundament of that discipline rests in single-phase flow, a brief introduction to the most usual fluid dynamic concepts will now be presented. For further details concerning single-phase flow the reader is directed to for example Schlichting [49].

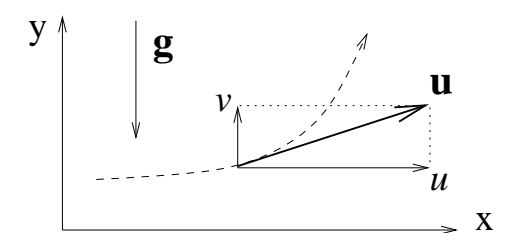


FIGURE 2.1. The velocity vector \mathbf{u} and the gravity \mathbf{g} .

The Navier-Stokes equations (NS), are together with the equations for continuity and energy the cornerstones of the continuum fluid dynamics. We will here focus on the NS and continuity equations, as the effects of heat generation and transport has been neglected in all included studies of this thesis. We will also restrict ourself to only consider two dimensions. The two main parameters describing the properties of a fluid is the density and the viscosity. If the density of the fluid is ρ and the viscosity is μ , conservation of mass and momentum is expressed explicitly by

$$\frac{\partial \rho}{\partial t} + \frac{\partial \rho u}{\partial x} + \frac{\partial \rho v}{\partial y} = 0 \quad (1)$$

$$\rho \frac{\partial u}{\partial t} + \rho \left(u \frac{\partial u}{\partial x} + v \frac{\partial u}{\partial y}\right) = X - p_x + \frac{\partial}{\partial x} \left[\mu \left(2 \frac{\partial u}{\partial x} - \frac{2}{3} \left(\frac{\partial u}{\partial x} + \frac{\partial v}{\partial y}\right)\right)\right] + \frac{\partial}{\partial y} \left[\mu \left(\frac{\partial u}{\partial y} + \frac{\partial v}{\partial x}\right)\right]$$
(2)

$$\rho \frac{\partial v}{\partial t} + \rho \left(u \frac{\partial v}{\partial x} + v \frac{\partial v}{\partial y}\right) = Y - p_y + \frac{\partial}{\partial x} \left[\mu \left(\frac{\partial u}{\partial y} + \frac{\partial v}{\partial x}\right)\right] + \frac{\partial}{\partial y} \left[\mu \left(2 \frac{\partial v}{\partial y} - \frac{2}{3} \left(\frac{\partial u}{\partial x} + \frac{\partial v}{\partial y}\right)\right)\right]$$
(3)

Here the velocity vector field is denoted by $\mathbf{u} = u\mathbf{e}_x + v\mathbf{e}_y$ as demonstrated in figure 2.1. Body forces X and Y in the momentum equations (2) and (3) are typically "external" forces on the fluid, from for example magnetic fields or, as in the papers included in this thesis, the gravity field: X = 0 and $Y = -\rho g\mathbf{e}_y$.

The boundary conditions connected to the governing equations (1-3) are quite straight-forward. Walls are usually modelled with no-slip conditions, i.e.

velocities parallel as well as normal to the wall are zero. Inlets are modelled with Dirichlet prescribed values for the velocities, and a convenient condition for the outlets is constant pressure and zero velocity gradients.

A convenient reorganisation of equations (2-3), used in several of the included articles, is to substitute the static pressure, p, with a reduced pressure, P, according to $P = \rho gy + p$. One advantage with this operation is the subsequent simple structure of boundary conditions for freely convected buoyant channel flow in vertical channels. The BC:S at the inlet and outlet become $P_{inlet} = P_{outlet} = 0$.

Together with the density and the viscosity, the characteristics of a flow is determined by the typical scales for velocity and length. For example, the rise velocity and the diameter of a rising gas bubble in water. The relative magnitude of the four parameters gives a first indication of the nature of the flow via the Reynolds number. While the flow out from a bottle of syrup is a highly viscous flow, the internal flow in a fast rotating water pump is the opposite.

Let U and L be typical values of the velocity and length. The ratio between the left hand side (the inertial contribution) and the last terms of the right hand side (the viscous contribution) of equations (2) and (3) can be estimated by

$$\frac{inertial\ forces}{viscous\ forces} \sim \frac{\rho U^2/L}{\mu U/L^2} = \frac{UL\rho}{\mu} = Re. \tag{4}$$

For further discussions about the Reynolds number and some other selected dimensionless parameters, the reader is directed to section 3, this chapter . A commonly appearing conception in the papers of this thesis is the one of Poiseuille flow. If we first rewrite equations (1-3) to the simpler form valid for steady state incompressible flow, i.e. $\rho = const$

$$\frac{\partial u}{\partial x} + \frac{\partial v}{\partial y} = 0 \tag{5}$$

$$u\frac{\partial u}{\partial x} + v\frac{\partial u}{\partial y} = -\frac{p_x}{\rho} + \frac{\mu}{\rho} \left[\frac{\partial^2 u}{\partial x^2} + \frac{\partial^2 u}{\partial y^2} \right]$$
 (6)

$$u\frac{\partial v}{\partial x} + v\frac{\partial v}{\partial y} = -\frac{p_y}{\rho} + \frac{\mu}{\rho} \left[\frac{\partial^2 v}{\partial x^2} + \frac{\partial^2 v}{\partial y^2} \right]$$
 (7)

and then apply the equations to laminar flow in a channel, as presented in figure 2.2, the developed velocity profile can easily be derived.

Let $\mathbf{u} = v(x)\mathbf{e}_y$ so that (5) and (6) cancel and neglect the inertial contribution in (7) which then yields

$$v(x) = -\frac{\partial p}{\partial y} \frac{(h-x)x}{2\mu}.$$
 (8)

Integration of the velocity over the channel leads to a useful expression for the constant pressure drop along a channel where the incompressible fluid travels laminarly with an average velocity V.

$$V = -\frac{1}{2\mu h} \frac{\partial p}{\partial y} \int_0^h (h - x) x dx \qquad \Rightarrow \qquad \frac{\partial p}{\partial y} = -\frac{12\mu V}{h^3} \tag{9}$$

The viscous flow in a channel with plane parallel walls are commonly known as *Poiseuille flow*. If the fluid, as indicated in figure 2.2, enters the channel with a uniform velocity, the inlet length necessary for the Poiseuille profile to develop is

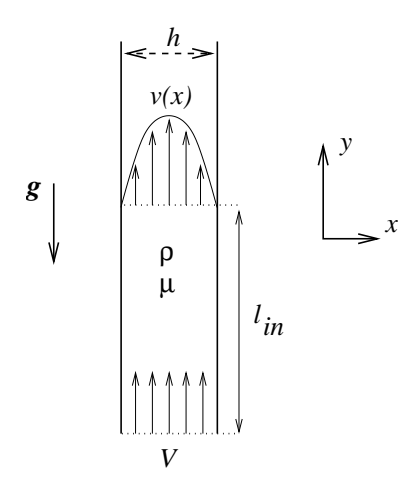


FIGURE 2.2. Development of a laminar Poiseuille velocity profile.

empirically given by [49]

$$l_{in} = \frac{h}{25} \frac{V \rho h}{\mu}.$$
 (10)

Finally, before ending this section, we will define two conceptions frequently encountered in the studies of this thesis. For the channel flow in figure 2.2 the shear rate $\dot{\gamma}$ is defined as

$$\dot{\gamma} = \frac{\partial v}{\partial x} + \frac{\partial u}{\partial y} \approx \frac{\partial v}{\partial x},\tag{11}$$

while the shear stress are expressed as

$$\tau = \mu \dot{\gamma} \approx \mu \frac{\partial v}{\partial x},\tag{12}$$

Upon the basic principles here given for single phase flow, we can now proceed with a discussion of two phase flow.

2. Two-Phase Flow

Let us start by defining some basic concepts. For further details the reader is directed to Hetsroni (1981) [23]. Local gas volume fraction or void fraction α is the portion of a local volume V which is occupied of gas,

$$\alpha = \frac{V_{gas}}{V_{gas} + V_{liq}}. (13)$$

The total fraction of phases are equal to one, so that $\alpha_{liq}=1-\alpha_{gas}$. If no subindice are explicitly written out, the meaning of the volume fraction α is always the gas volume fraction. The volume flux ratio is the ratio of the gas volume-flow rate Q_{gas} to the total volume-metric flow rate $Q_{gas}+Q_{liq}$,

$$\beta = \frac{Q_{gas}}{Q_{gas} + Q_{liq}}. (14)$$

If there is a relative velocity between the two phases, the void fraction and the flux ratio are not equal $\alpha \neq \beta$. Another important concept is the superficial velocity j which is the velocity of a phase based on its flux rate Q,

$$j_{gas} = \frac{Q_{gas}}{A} = \frac{1}{A} \int_{A} \alpha v_{gas} dA, \qquad j_{liq} = \frac{Q_{liq}}{A} = \frac{1}{A} \int_{A} (1 - \alpha) v_{liq} dA \quad (15)$$

where A is the local cross-sectional area for the stream tube and v is the separate velocity for each phase. As we in the papers solely deal with bubbly flows, we will there mostly use the notation j_d and j_c for the dispersed gas phase and the continuous liquid phase respectively. Note that both α and β are local values that varies over the cross-section of a channel. Alternatively it is also possible to discuss the total void fraction (gas hold up) or the total flux ratio in a large area or section. It is in those situations clearly indicated.

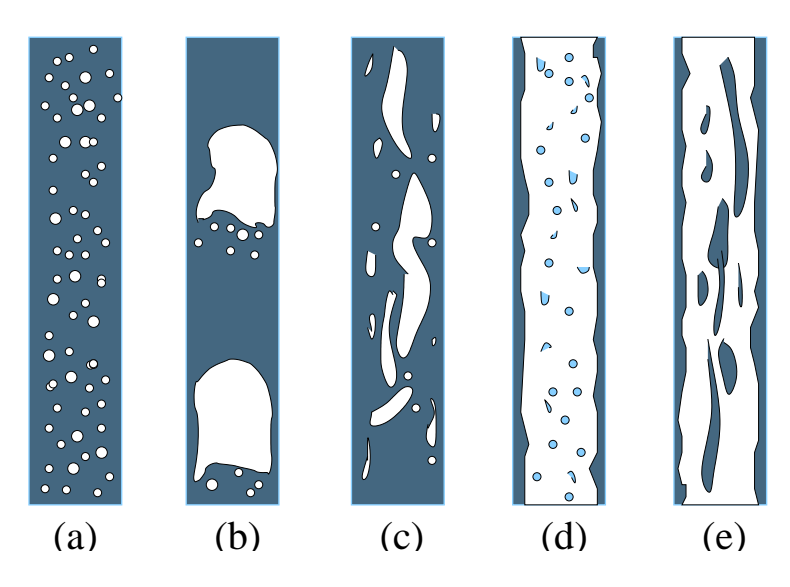


FIGURE 2.3. Two phase vertical upward flow patterns.

For a successful modelling of two-phase flow, the first compulsory step is to characterise the flow. Although not completely equivalent, vertical pipe flow can be used for a short guide on this matter, [24]. The main flow regimes, as illustrated in figure 2.3, are then:

- (a) Bubbly flow with low rate of coalescence.
- (b) Slug flow which appear when the volume flux ratio of gas is increased. Bubbles start to coalesce and form larger elongated bubbles, reaching over the width of the channel separated by liquid slugs.
- (c) Churn flow appears if the volume flux ratios from (b) is remained with increased flux for both phases.
- The liquid slugs become unstable and break up in an oscillating fashion.
- (d) Annular flow, where the gas travel in the mid of the pipe with a high superficial velocity.
- (e) Wispy annular flow for high mass velocities.

In this study we will restrict ourself to the bubbly regime, with a complete negligence of bubble coalescence. Primarily two different mathematical models are then close to hand for the modelling of the bubbly two-phase flow when the number density is too large to make individual tracking practical. The first option is the "Two-Fluid" model which request one set of conservation equations for each phase, i.e. six equations for a 2D problem. Interfacial exchange of drag, mass etc. are described by more or less empirical closure relations. The second possible option is known under the names "Mixture", "diffusion" or "drift flux" model. This two-phase model is attractive because of its simplicity. In the mixture model the closure laws request a direct implementation of the relative velocity between the phases. For a 2D problem it is hence sufficient to solve four equations.

Restricted to the bubbly regime, or in our case rather the mono-dispersed suspension regime, we will in what follows as much as possible use a notation where subindice d and c represent the dispersed phase (gas bubbles) and the continuous phase (fluid). It is further assumed that the rise velocity U_s for a single bubble of radius a, (figure 2.4) can be predicted by the Stokes terminal rise velocity of a sphere, modified for a bubble [54]

$$U_s = \frac{ga^2\rho_c}{3\mu_c} \tag{16}$$

The important (non-dimensional) Bubble Reynolds number can now be defined as

$$Re_b = \frac{U_s 2a\rho_c}{\mu_c} \tag{17}$$

A brief description of the two models with necessary definitions will be given next.

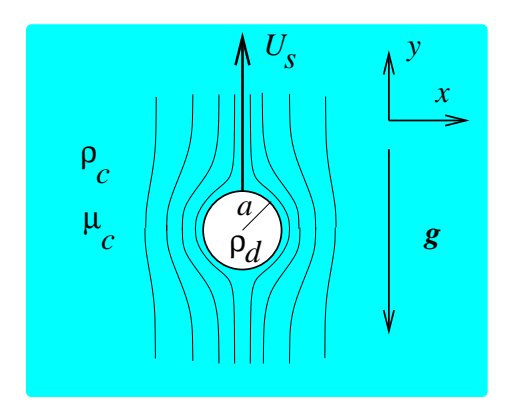


FIGURE 2.4. A single bubble of radius a laminarly rising in liquid.

2.1. The Two-Fluid Model.

Let the sub-indices d and c denote the dispersed and the continuous phase respectively so that ρ_d , ρ_c , μ_d , μ_c , P_d , P_c , and \mathbf{u}_d , \mathbf{u}_c are the density, viscosity, pressure and velocity for the dispersed and continuous phase respectively. The void fraction for gas and liquid though are expressed by α and $(1 - \alpha)$. Under

the assumption that the local balance equations (1-3) are time averaged for each phase, the stationary mass and momentum equations for the two-fluid model is written:

Dispersed Phase

$$\nabla \cdot (\alpha \rho_d \mathbf{u}_d) = 0 \tag{18}$$

$$\alpha \rho_d \mathbf{u}_d \cdot \nabla \mathbf{u}_d = \alpha (\rho_d \mathbf{g} - \nabla p_d) + \nabla \cdot (\alpha \mu_d [\nabla \mathbf{u}_d + \nabla \mathbf{u}_d^T]) - \mathbf{M}, \tag{19}$$

Continuous Phase

$$\nabla \cdot ((1 - \alpha)\rho_c \mathbf{u}_c) = 0 \tag{20}$$

$$(1 - \alpha)\rho_c \mathbf{u}_c \cdot (\nabla \mathbf{u}_c) = 0$$

$$(1 - \alpha)\rho_c \mathbf{u}_c \cdot (\nabla \mathbf{u}_c) = (1 - \alpha)(\rho_c \mathbf{g} - \nabla p_c) +$$

$$\nabla \cdot ((1 - \alpha)\mu_c [\nabla \mathbf{u}_c + \nabla \mathbf{u}_c^T]) + \mathbf{M}.$$
(21)

The boundary conditions connected to the governing equations are for each phase equal to those used in single-phase flow modelling. The void fraction is conveniently specified at the inlet.

Even though the pressure inside a bubble can be higher than the static pressure of the fluid due to surface tension, the pressure on the bubbles, from a macro point of view, is the actual pressure of the liquid. A simple assumption which is commonly adapted is therefore

$$p_d = p_c = p. (22)$$

The last terms in equations (19) and (21) model the interfacial momentum transfer. In order to solve the averaged balance equations of the two fluid system, closure laws has to be provided for these terms. The interfacial momentum transfer is usually divided into several different parts [29], each contributing with drag, lift, virtual mass forces and interfacial pressure etc.

$$\mathbf{M} = \mathbf{M}^D + \mathbf{M}^L + \mathbf{M}^{VM} + \mathbf{M}^P \tag{23}$$

These forces are for dilute flow, obtained from the force on one single isolated bubble and then averaged over the mixture.

• The Drag Term

The first contribution to the momentum transfer as expressed in equation 23 is the drag term. This term is for a suspension easily derived starting from the drag on one single bubble

$$\mathbf{D}_{p} = \frac{1}{2} \rho_{c} C_{D} A_{p} \mid \mathbf{u}_{r} \mid \mathbf{u}_{r} \tag{24}$$

where C_D is the drag coefficient, $A = \pi a^2$ is the projected area of a bubble and $\mathbf{u}_r = \mathbf{u}_d - \mathbf{u}_c$ is the relative velocity of the phases. If now $V_p = 4\pi a^3/3$ is the volume of one bubble, the total number of number of bubbles in a unit volume of the fluid is

$$n_p = \frac{\alpha}{V_p} = \frac{3\alpha}{4\pi a^3}. (25)$$

The total drag between the phases in a unit volume of the suspension can hence be derived by taking $\mathbf{M}^D = n_p \mathbf{D}_p$

$$\mathbf{M}_{p} = \frac{3}{8} \frac{\alpha C_{D}}{a} \rho_{c} \mid \mathbf{u}_{r} \mid \mathbf{u}_{r}. \tag{26}$$

The drag coefficient C_D depends on the characteristics of the flow, and is usually divided in four distinct regimes

- (i) The Stokes Regime, $(Re_b \leq 0.2)$: $C_D = \frac{24}{Re_b}$ This expression is valid in the limit $Re_b \rightarrow 0$ where the drag is due to skin friction.
- (ii) The Allen Regime, $(Re_b \le 500 1000)$: $C_D = \frac{24}{Re_b}(1 + 0.15Re_b^{0.687})$ Both skin friction and the form drag is important.
- (iii) The Turbulent Regime, $(500-1000 \le Re_b \le 1-2\cdot 10^5)$: $C_D=0.44$ Form drag dominates.
- (iv) The supercritical Regime, $(Re_b \ge 1-2\cdot 10^5)$: $C_D=0.1$ Form drag dominates and the boundary layer around the sphere changes from laminar to turbulent.

The standard drag curve of Ihme et al. [28] is commonly used. The drag is, expressed by this function, represented for all Reynolds numbers up to the critical $Re_{b,crit} = 1 - 2 \cdot 10^5$, where the drag suddenly drops. As the bubble Reynolds number in the present work is estimated to be in the order of unity or less, the relevant regime is the Stokes regime. The standard drag curve are displayed in figure 2.5 together with the other drag terms.

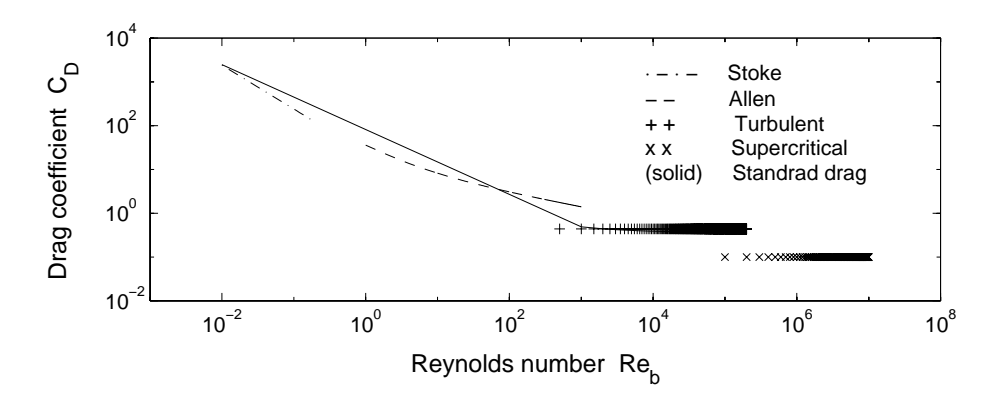


FIGURE 2.5. The drag coefficient for a spheric particle.

ullet The Lift Term

The lift force can be expressed by e.g.

$$\mathbf{M}^{L} = C_{L} \rho_{c} \alpha \mathbf{u}_{r} \times (\nabla \times \mathbf{u}_{c}) \tag{27}$$

where C_L is the lift coefficient, ([3], [19]). In the presence of a wall, a correction exists according to [33]. Lance suggests the value $C_L = 0.25$ for the lift coefficient. In the two-fluid model study performed in paper 1 (this thesis), no lift force is considered.

• The Virtual Mass Force

The virtual mass force is defined

$$\mathbf{M}^{VM} = C_{VM} \alpha \rho_c \mathbf{a}_{VM} \tag{28}$$

where the virtual mass acceleration according to Drew [19] is

$$\mathbf{a}_{VM} = \left(\frac{\partial}{\partial t} + \mathbf{u}_d \cdot \nabla\right) \mathbf{u}_d - \left(\frac{\partial}{\partial t} + \mathbf{u}_c \cdot \nabla\right) \mathbf{u}_c \tag{29}$$

The virtual mass acceleration is not considered in the two-fluid model study performed in paper 1 (this thesis).

• The Interfacial Pressure Term

The interfacial pressure term is expressed by

$$\mathbf{M}^p = (p_{ci} - p_c)\nabla(1 - \alpha) + p_c\nabla(1 - \alpha). \tag{30}$$

Here $(p_{ci} - p_c) = C_p \rho_c \alpha_c \mid \mathbf{u}_r \mid^2$ and p_c is the bulk liquid pressure. For potential flow around a sphere the pressure coefficient is $C_p = 0.25$, [32]. A usual choice is to neglect this term. This is also the case in paper 1 (this thesis).

2.2. The Mixture Model.

In the papers 2, 5 and 6 of this thesis we have used a mixture model formulation of Ishii [29] for the dispersal of particles in a suspension. Since we solely deal with small bubbles ($a \sim 10^{-5} \ m$) it is hence a necessary assumption that the physical properties of these bubbles can be compared to particles. in the developing channel flow. This assumption is somewhat justified as the bubble Reynolds number ($Re_b \sim 1$) is of order unity and the Weber, Bond and Capillary numbers are all small (10^{-1} or less). The bubbles are consequently expected to remain spherical and to behave as particles.

Assume that the mixture has Newtonian properties which depend on the local void fraction α . Let $\rho_d \ll \rho_c$ be the densities of the dispersed and continuous phase and $\mu_d \ll \mu_c$ the viscosities. For the mixture it is then possible to write the effective density

$$\rho = \alpha \rho_d + (1 - \alpha)\rho_c \approx (1 - \alpha)\rho_c, \tag{31}$$

and the effective viscosity as formulated by Ishii & Zuber [30]

$$\mu = \mu_c (1.0 - \frac{\alpha}{\alpha_m})^{-2.5\alpha_m \frac{\mu_d + 0.4\mu_c}{\mu_d + \mu_c}} \approx \frac{\mu_c}{1 - \alpha}$$
 (32)

Here $\alpha_m \approx 1$ is the maximum possible void fraction of gas. The unity value is chosen due to simplicity and it should be noted that a maximum possible packing rate for spheres is limited to $\alpha_m \approx 0.68$

Now let \mathbf{u}_d and \mathbf{u}_c be the separate velocities of the two phases, i.e. the actual velocity with which a bubble or an element of the fluid travel as experienced by an external observer. The superficial velocities, equation (15) then writes

$$\mathbf{j}_d = \alpha \mathbf{u}_d, \qquad \mathbf{j}_c = (1 - \alpha) \mathbf{u}_c \tag{33}$$

which, summed for the mixture, yields

$$\mathbf{j} = \mathbf{j}_d + \mathbf{j}_c. \tag{34}$$

The motion of the dispersed phase relative to the mixture can now be defined in a practical manner via the volume flux density vector

$$\mathbf{j}_r = \mathbf{j}_d - \alpha \mathbf{j}. \tag{35}$$

As now drag terms between the phases is involved in the same manner as in the two-fluid model, the closure of the mixture model demands a direct input of the relative flux \mathbf{j}_r . The explicit definition of \mathbf{j}_r can however still include a dependence of phase velocities, shear rate and local void.

If a mass averaged velocity vector **q** for the mixture is averaged as

$$\rho \mathbf{q} = \rho_d \mathbf{j}_d + \rho_c \mathbf{j}_c, \tag{36}$$

the relation between **j** and **q** are in the limit $\rho_c >> \rho_d$ expressed as

$$\mathbf{j} = \mathbf{q} - \frac{(\rho_d - \rho_c)/\rho_c}{(1 + (\rho_d - \rho_c)/(\rho_c)\alpha)} \mathbf{j}_r \approx \mathbf{q} + \frac{1}{(1 - \alpha)} \mathbf{j}_r.$$
(37)

Two-phase mathematical modelling based on the mixture formulation has been used is papers 2, 5 and 6. In these studies, a closure of the system has been performed using empirical laws for the definition of the relative volume flux

$$\mathbf{j}_r = \mathbf{j}_s + \mathbf{j}_{diff} + \mathbf{j}_{coll} + \mathbf{j}_{saff}. \tag{38}$$

These laws are originally developed for particle sedimentation in suspensions. The first term on the r.h.s. of equation (38) is a relative motion parallel to the walls, while the other terms essentially have their largest components perpendicular to the walls.

A brief discussion of the origin of these relations, for the most part based on mutual interactions between bubbles, is given next. The notation will follow the definitions given previously, such as $\dot{\gamma}$ for the shear rate (equation 11), τ for the shear stress (equation 12), and U_s for the rise velocity of a single bubble (equation 16). The coordinate system is indicated in figures 2.2 and 2.4. For a complete understanding, the hindering function here given the formulation [30] of Ishii & Zuber

$$f(\alpha) = (1 - \alpha)\mu/\mu_c = (1 - \alpha)^2 \tag{39}$$

must also be introduced. This is a correlation to the rise velocity of a single bubble, invoking the properties of the effective density and viscosity for the mixture.

• Buoyancy Induced Vertical Rise

$$\mathbf{j}_s = \alpha U_s f(\alpha) \mathbf{e}_y, \tag{40}$$

Besides the convection, the main contribution to the flux in the vertical direction, parallel to the gravity (figure 2.2), is the relative volume flux density \mathbf{j}_s , [17], directly caused by buoyancy.

 $\bullet \ The \ Hydrodynamic \ Self \ Diffusion$

$$\mathbf{j}_{diff} = -aU_s f(\alpha) \left[D_{\perp} \frac{\partial}{\partial x} \alpha \mathbf{e}_x + D_{\parallel} \frac{\partial}{\partial y} \alpha \mathbf{e}_y \right]$$
 (41)

Nicolai et al. [42] quantified the fluctuating velocity components of sedimenting particles in an otherwise quiescent suspension. It is here assumed that the same empirical relations for the diffusive process will hold for tiny spherical bubbles. The magnitude for this process is stronger in the direction parallel to the rise path of the gas bubbles, $(D_{\perp} \approx 1, \ D_{\parallel} \approx 8)$.

• The Shear Induced Hydrodynamic Diffusion and Migration

$$\mathbf{j}_{coll1} = -a^2 \dot{\gamma} \beta(\alpha) \nabla \alpha, \tag{42}$$

$$\mathbf{j}_{coll2} = -a^2 \dot{\gamma} \frac{\kappa(\alpha)}{\tau_{xy}} \nabla \tau_{xy} \tag{43}$$

These diffusion processes, induced by the shear of the mixture and described by [34] and [48] are assumed to be caused by the interactions of particles with an average displacement, a, and an interaction frequency which is proportional to the magnitude of the shear rate, equation (11). The empirical functions $\beta(\alpha)$ and $\kappa(\alpha)$ are given by [12] and [34] and formulate as

$$\beta(\alpha) = \frac{1}{3}\alpha^2 (1 + 0.5e^{8.8\alpha}),\tag{44}$$

$$\kappa(\alpha) = 0.6 \,\alpha^2. \tag{45}$$

• The Saffman Lift Effect

$$\mathbf{j}_{saff} = -\alpha f(\alpha) \frac{6.46}{6\pi} U_s \sqrt{\frac{a^2 \rho_c}{\mu_c} |\dot{\gamma}|} sgn(\frac{\partial v}{\partial x}) \mathbf{e_x}$$
(46)

This expression is valid for small particles in shear flow and describes lateral migration due to a force emanating from the difference in pressure around a non-neutral buoyant particle moving in shear flow, [47]. The expression is valid for low bubble and shear Reynolds number $Re_b \ll \sqrt{Re_{\dot{\gamma}}} < 1$ where the shear Reynolds number is defined as

$$Re_{\dot{\gamma}} = \frac{\dot{\gamma} 4a^2 \rho_c}{\mu_c} \tag{47}$$

The validity of (46) was extended by McLaughlin [38] so that bubble Reynolds numbers higher than the shear Reynolds number was allowed. Contributions on this matter are given also by Mei [39].

Other potential contributions modelling the drag or lift of bubbles can be mentioned. None of those are however included in the studies which are presented in the papers of this thesis. One example of such contributions could be the Magnus force. Others are for example the Faxén force [27], the virtual mass effect and the Basset force [15].

• The Magnus Force

$$\mathbf{F}_{mag} = -\pi a^3 \rho_c \left[\left(\frac{1}{2} \nabla \times \mathbf{u}_c - \omega \right) \times (\mathbf{u}_d - \mathbf{u}_c) \right]$$
 (48)

which for bubbly flow in vertical channels give rise to a lateral velocity

$$\mathbf{j}_{mag} = \frac{\alpha f(\alpha) U_s a^2}{6\nu_c} \mathbf{e}_x (\omega - \frac{v_x}{2}) \tag{49}$$

Here \mathbf{u}_c and \mathbf{u}_c are true velocities of the dispersed and continuous phases respectively. Due to the rotation ω of the particle a pressure difference is established between both sides of the particle [45]. The rotation may be caused by the shear rate but also of other reasons. The relation is valid for a bubble Reynolds number of the order of unity.

The governing equations

The governing equations of the mixture model are

$$\nabla \cdot \mathbf{j} = 0, \tag{50}$$

$$\nabla \cdot \mathbf{j}_d = 0, \tag{51}$$

$$\nabla \cdot \mathbf{j}_{d} = 0, \qquad (51)$$

$$\rho \mathbf{q} \cdot \nabla \mathbf{q} = -\nabla p + \mathbf{g} \rho + \nabla [\mu (\nabla \mathbf{q} + \nabla \mathbf{q}^{T}) - (\frac{2}{3} \mu \nabla \cdot \mathbf{q})] \qquad (52)$$

and they assure the conservation of volume of the two incompressible phases and the momentum of the mixture. The equations (50-51) can now, for convenience, be reformulated by using the previously defined relations (34-37). Note that the necessary assumption is still that $\rho_d \ll \rho_c$. It is also convenient to introduce the reduced pressure $P = p + \rho_c gy$. The new set of governing equations are then

$$\nabla \cdot [(1 - \alpha)\mathbf{q}] = 0, \tag{53}$$

$$\nabla \cdot \left[\alpha \mathbf{q} + \frac{1}{1 - \alpha} \mathbf{j}_r \right] = 0, \tag{54}$$

$$\rho \mathbf{q} \cdot \nabla \mathbf{q} = -\nabla P + \alpha \rho_c g \mathbf{e}_y + \nabla [\mu (\nabla \mathbf{q} + \nabla \mathbf{q}^T) - (\frac{2}{3}\mu \nabla \cdot \mathbf{q})]$$
(55)

The boundary conditions

No-slip boundary conditions for the mass averaged velocity \mathbf{q} are used on all walls. Inlet conditions are modelled with prescription of the inlet values for void fraction α and mass averaged velocities q. Outlets are modelled with prescription of the pressure p. Gas producing walls are slightly more complicated to model. Combining equations 34 with 35 and using that $\mathbf{j}_d \cdot \mathbf{n} = j_{gas}$ and $\mathbf{j}_c \cdot \mathbf{n} = 0$ where j_{gas} is the production velocity of the gas, the boundary condition at the gas producing wall is

$$\mathbf{j}_r \cdot \mathbf{n} = (1 - \alpha) j_{gas}. \tag{56}$$

3. Some Dimensionless Parameters

As previously mentioned, the characteristics of a flow is conveniently described in terms of non-dimensional parameters. Restricting ourself to a dispersed two-phase flow under constant temperature, some of the most useful dimensionless number are summarised in what follows.

Let V be a representative velocity, L a typical length scale and ν_c and ρ the density and viscosity for the liquid. The ratio between inertial and viscous forces for a unit volume of the liquid is then

$$\frac{Inertial\ force}{Viscous\ force} \sim \frac{\rho_c \nabla V^2}{\mu_c \nabla^2 V} \qquad \Rightarrow \qquad Re = \frac{VL}{\nu_c} \tag{57}$$

also known as the Reynolds number. This parameter effectively measures whether the liquid flows laminarly $(Re < Re_{crit})$ or turbulent $(Re > Re_{crit})$. Generally, the transition to turbulence occurs for Reynolds number roughly in the order of $Re_{crit} \sim 10^3$ for channel flow $(L = Channel\ width,\ V = Mean\ velocity)$.

Alternative formulations of the this parameter are achieved if for example the representative velocity is the rise velocity U_s of a bubble and the length scale is given by the bubble diameter 2a:

$$\frac{Inertial\ force}{Viscous\ force} \sim \frac{\rho_c \nabla U_s^2 (4\pi a^3/3)}{\mu_c \nabla^2 U_s (4\pi a^3/3)} \qquad \Rightarrow \qquad Re_{2a} = \frac{U_s 2a}{\nu_c}. \tag{58}$$

This parameter is known as the bubble Reynolds number and its importance is partly described in section 2.1.

For shearing flow, a third variant of the Reynolds number is formulated. Let the bubble diameter 2a be the length scale and the velocity drop $(\dot{\gamma}2a)$ over this length be the velocity scale. The shear Reynolds number is then

$$\frac{Inertial\ force}{Viscous\ force} \sim \frac{\rho_c \nabla (\dot{\gamma} 2a)^2 (4\pi a^3/3)}{\mu_c \nabla^2 (\dot{\gamma} 2a) (4\pi a^3/3)} \qquad \Rightarrow \qquad Re_{\dot{\gamma}} = \frac{\dot{\gamma} (2a)^2}{\nu_c}. \tag{59}$$

The shear Reynolds number replace for example the role of the bubble Reynolds number for a neutral buoyant particle with zero bubble Reynolds number.

Three important dimensionless parameters in bubbly flows are the Weber number ${\bf v}$

$$\frac{Inertial\ force}{Surface\ tension force} \sim \frac{\rho_c U_s \nabla U_s (4\pi a^3/3)}{\sigma 2\pi a} \quad \Rightarrow \quad We = \frac{\rho_c U_s^2 2a}{\sigma}, \tag{60}$$

the Eötvös number or Bond number

$$\frac{Gravitational\ force}{Surface\ tension\ force} = \frac{\Delta \rho_c g(4\pi a^3/3)}{\sigma^2 \pi a} \qquad \Rightarrow \qquad Eo = Bo = \frac{\Delta \rho g(2a)^2}{\sigma} \ (61)$$

and the capillary number

$$\frac{Viscous\ force}{Surface\ tension\ force} \sim \frac{\mu_c \nabla^2 U_s(4\pi a^3/3)}{\sigma 2\pi a} \qquad \Rightarrow \qquad Ca = \frac{\mu_c U_s}{\sigma}. \tag{62}$$

By measuring the ratios between surface tension force on one hand and inertial, gravitational or viscous forces on the other, it is possible to estimate whether the bubble will deform in the flow or remain spherical. A small ratio indicates that the surface tension is large enough to resist the deforming forces. In the present thesis the bubble radius is typically $a \sim 10^{-5}$ (m) and the relative velocity is $U_s \sim 10^{-2}$ (m/s). Using the value for surface tension of water $\sigma \approx 7 \cdot 10^{-5}$ (N/m) the Weber, Eötvös and Capillary numbers thus are 10^{-1} or less. Our assumption that the bubbles remain spherical should consequently be justified.

CHAPTER 3

Basic Electrochemical Concepts

1. Reaction Kinetics at Electrodes

Electrochemistry involves the inter-conversion of chemical and electrical energy. For a detailed description of this subject, the reader is advised to Bockris & Reddy (1977) ([7], [8]), Newman (1991) [41], or Walsh (1993) [56]. The reactions occur at the electrodes which are surrounded by electrolyte. A fundamental electrochemical cell can belong to one of two contradictory cases;

- (i) The *galvanic cell* in which electrochemical energy spontaneously is conversed into electrical energy. Examples of galvanic cells are batteries of different kinds and fuel cells.
- (ii) The *electrolytic cell* in which a potential difference, exceeding the equilibrium difference, is applied between two electrodes separated by electrolyte. Electrical energy is hence conversed to chemical energy. This cell is conceptual in the electrochemical industry which often consumes large amounts of electric power. The purpose of the process is to change the character of an electrolyte or the surface of one or both of the electrodes involved in the reactions.

The work of this thesis consider solely electrolytic cells, more or less inspired from conceptual industrial processes. 1

Faraday stated already in the nineteenth century the first and the second Laws of Electrolysis. These laws form a base upon which we then can discuss the details of the reaction kinetics.

Faradays first law: The substance mass generated by an electrolytic reaction is proportional with the amount of electricity passed through the cell,

Faradays second law: One equivalent weight of a substance is generated at each electrode during the passage of 96485 coulomb of charge 2 through an electrolytic cell.

A brief discussion will here follow which exemplifies the kinetics at an electrode. Industrial electrodes exist in several forms and material. The shape can be flat, rounded or even porous. Normally, the material of the electrodes are well conducting solid metals or carbon, but also polymers and ceramics and even

¹ Paper 1 and 2 consists of studies mainly focused on the chlorate process.

²The Faradays number is equivalent to $F = 96485 \ C/mole$

floating matters are in use. We will however restrict this discussion as well as the performed studies of this thesis to plane metal electrodes in parallel pairs separated by a channel filled with electrolyte.

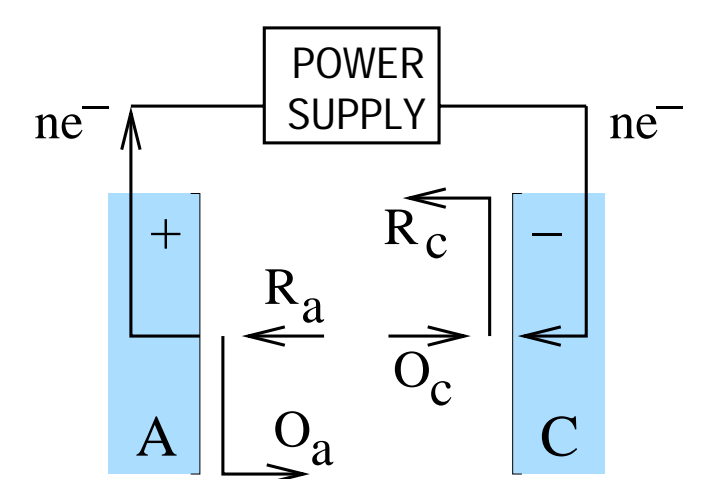


FIGURE 3.1. Kinetics in an electrolytic cell- Anodic oxidation of R_a and cathodic reduction of O_c .

The reactions occurring at the electrodes in an electrolytic electrochemical cell can be schematically written as

At the anode	$R_a - ne^- \rightarrow O_a$
At the cathode	$O_c + ne^- \rightarrow R_c$
Totally in the cell	$O_c + R_a \rightarrow O_a + R_c$

where R and O are the reduced and oxidised species respectively, also demonstrated in figure 3.1. As an electric current now is pumped from the cathode to the anode via the power supply, an equal amount of current must flow in the electrolyte. This occurs by a flux of charged ions; the positive cations to the cathode and negative anions to the anode. The total reaction reveals the end product of the process. In many industrial processes, which could include combined reactions of several species, the necessary reactants is consumed after some time of running. The electrolyte must then be replaced, either continuously or instantly.

Let a system with electrolysis of water, figure 3.2a illustrate a simple but conceptual electrolytic cell. A potential difference is applied between the anode and the cathode. The electrolyte can for example consist of NaOH solved in water. Here the OH^- ions take part in the electrode reactions while the Na^+ ions solely have a supporting role in the electrolyte.

The cathodic reduction of water occurs by

$$4H_2O + 4e^- \rightarrow 4OH^- + 2H_2(gas)$$
 (63)

and the anodic oxidation of hydroxide ions according to

$$4OH^- \to O_2(gas) + 4e^- + 2H_2O.$$
 (64)

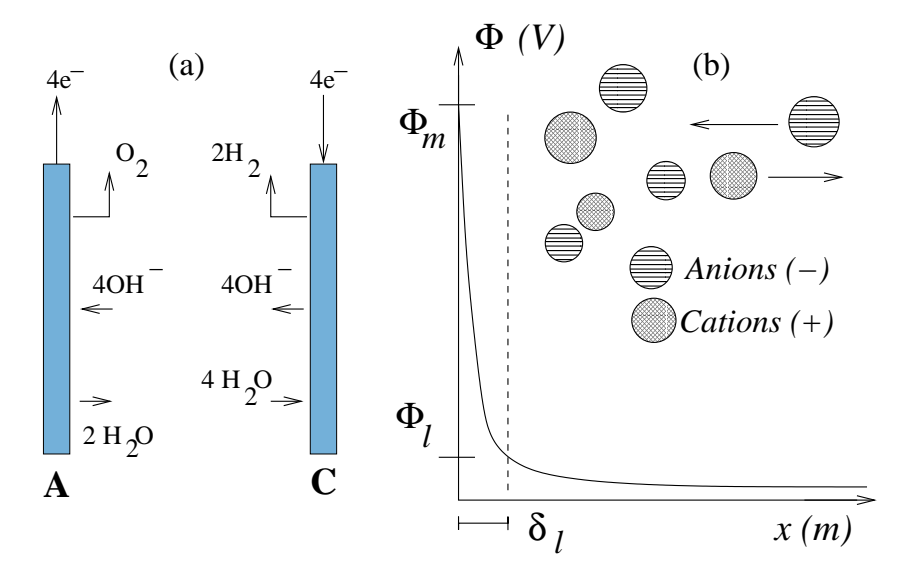


FIGURE 3.2. (a) The electrode reactions in water electrolysis. (b) Schematic sketch over the electric double layer adjacent to an anode.

As the total reaction for the system we have

$$4H_2O + 4e^- + 4OH^- \rightarrow 4OH^- + 2H_2(gas) + O_2 + 4e^- + 2H_2O.$$
 (65)

$$\Rightarrow 2H_2O \to O_2(gas) + 2H_2(gas). \tag{66}$$

Water is hence consumed and converted into one part of oxygen gas and two parts of hydrogen gas. By using Faradays laws of electrolysis, the gas production rate for the reactions (63) and (64) can now be computed:

The produced mass is proportional to the amount of passed charge Q: First the current has to be defined;

$$Q = \int_{t_0}^{t_1} I dt \quad (= It)$$
 (67)

where the last approximation holds for a current which is constant in time, an assumption which for simplicity is made here.

One equivalent weight of a substance is generated for each 96485 coulomb of charge: It is, for example, evident from the reaction (64) that one oxygen molecule is produced for every n=4 electrons. It is hence possible to write

$$m = Q/nF \qquad (mole) \tag{68}$$

where m is the amount of produced substance (oxygen gas molecules) in mole and F = 96485 (C/mole). We now invoke equation (67) in (68) which then yields

$$m = \frac{It}{nF} \qquad (mole) \tag{69}$$

Now introduce the molar weight M (kg/mole) and the density ρ (kg/m^3) for the produced substance, define the current density i

$$i = I/A \qquad (A/m^2). \tag{70}$$

and further reformulate equation (68)

$$m = \frac{It}{nF} (mole) \qquad \Rightarrow \qquad \frac{m}{t} = \frac{I}{nF} (mole/s) \qquad \Rightarrow$$

$$\frac{mM}{t\rho} = \frac{IM}{nF\rho} (m^3/s) \qquad \Rightarrow \qquad \frac{mM}{At\rho} = \frac{IM}{AnF\rho} (m/s) \qquad \Rightarrow$$

$$j_{gas} = \frac{iM}{nF\rho} (m/s). \tag{71}$$

The superficial velocity (previously defined in (15) can for the anodic $(M_{O_2}, \rho_{O_2}, n=4)$ and cathodic $(M_{H_2}, \rho_{H_2}, n=2)$ reactions be computed as

$$j_{O_2} = \frac{iM_{O_2}}{4F\rho_{O_2}} (m/s), \qquad j_{H_2} = \frac{iM_{H_2}}{2F\rho_{2_2}} (m/s),$$
 (72)

It turns out that the formula (71) is a very useful result in the modelling of gas-evolving electrodes.

For electrolytic cells, the driving force of the electrode reactions is the potential gradient over the cell. In the immediate vicinity of the electrode (figure 3.2b), where the electron transfer take part, the potential gradient suddenly become very steep.³ This thin zone is commonly known as the electric double layer, and typical dimensions are given by molecular distances $\delta_l \sim 10^{-9} \ m$. In the figure, Φ_m and Φ_s denote the electric potential of the electrode and of the adjacent solvent respectively.

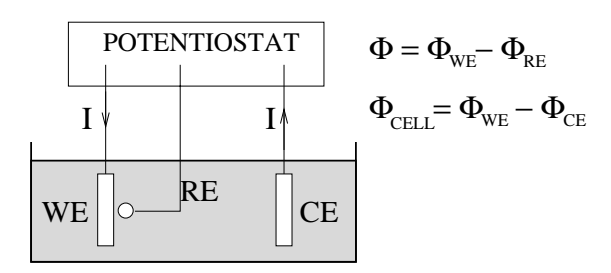


FIGURE 3.3. Working electrode, counter electrode and reference electrode. Three electrode system used to consider the kinetics at an working electrode.

In order to illustrate the theoretical relationship between current and voltage at a working electrode in an electrochemical cell, the setup in figure 3.3 will be

 $^{^3}$ For a conceptual industrial cell the potential difference between anode and cathode may by 10 V over 1 cm electrolyte gap giving a potential gradient of 10^3 V/m. This can be compared to a typical voltage drop of 1 volt over the double layer $\delta \sim 10^{-9}$ m giving a potential gradient of 10^9 V/m, i.e. 10^6 times higher than the drop in the electrolyte.

used. If now the potential over the cell itself is the difference in potential between the working electrode and the counter electrode 4

$$\Phi_{CELL} = \Phi_{CE} - \Phi_{WE},\tag{73}$$

the potential difference Φ over the electric double layer adjacent to the working electrode is commonly discussed in terms of a relative measure to the potential of a third (reference) electrode Φ_{RE} ⁵

$$\Phi = \Phi_{WE} - \Phi_{RE}. \tag{74}$$

It is now assumed that the only reaction at the working electrode is an interconversion between oxidised and reduced species according to

$$O + ne^- \rightleftharpoons R.$$
 (75)

This two-way traffic give rise to a simultaneous anodic and cathodic current density \overrightarrow{i} and \overleftarrow{i} , and the total current density is hence defined as the sum of the current densities from oxidation and reduction:

$$i = \overrightarrow{i} + \overleftarrow{i}. \tag{76}$$

If no net current runs over the electric double layer, $i = \overrightarrow{i} + \overleftarrow{i} = 0$, the concentrations of O and R remain constant and the potential difference over the layer will be the so called equilibrium potential

$$\Phi_e = \Phi_e^{\ominus} + \frac{RT}{nF} ln(\frac{c_O}{c_B}) \tag{77}$$

where Φ_e^{\ominus} is the tabulated standard equilibrium potential for the couple O/R. In this case the partial anodic and cathodic current densities are equal and the magnitude of the currents is known as the exchange current density

$$i_0 = -\overrightarrow{i} = \overleftarrow{i}$$
. (78)

In industrial applications are though the current density far from zero and the potential difference E over the electric double layer consequently not in equilibrium. These non-equilibrium situations are described in terms of the overpotential η on the working electrode, a property which is defined as

$$\eta = \Phi - \Phi_e, \tag{79}$$

i.e. the overpotential η is zero if the net current i is zero.

We now have all necessary definitions to express the full relation between the current density and the potential difference over the double layer, the Butler-Volmer equation

$$i = i_0 \left[e^{\frac{\alpha_A nF}{RT} \eta} - e^{-\frac{\alpha_C nF}{RT} \eta} \right]. \tag{80}$$

Here α_A and α_C are transfer coefficients for the anodic and cathodic processes. Note that $\alpha_A + \alpha_C = 1$ and that generally $\alpha_A = \alpha_C = 1/2$. Further is $R = 8.314 \ (VAs/K)$ the gas constant, $F = 96485 \ (As/mole)$ the Faraday constant, and n the number of electrons involved.

In most industrial processes, such a high cell-voltage is applied that either the

 $^{^4\}mathrm{The}$ concept potential is not a physical property in it self and can only be discussed as a relative measure

⁵The reference electrode has a well-established and reproducible potential independent of current density, such as the standard hydrogen electrode (SHE) which under standard conditions has a potential equal to zero. This form the basis of tabulated standard electrode potentials. Standard conditions here has the meaning that pure materials are used in their standard state, the hydrogen pressure is 1 atm. and the proton activity is 1.

right or left hand terms of the Butler-Volmer equation can be neglected; the relation is then generally known as the Tafel law. For an electrolytic cell $(\eta > 0)$ with such high over-voltage at the anode the Tafel law is expressed as

$$i = i_0 e^{\frac{\alpha_A \, nF}{RT} \eta}. \tag{81}$$

Using the relations and definitions in (74), (77) and (79) we may reformulate (81) as

$$i = i_0 e^{\frac{\alpha_A nF}{RT} \eta} =$$

$$i_0 e^{\frac{\alpha_A nF}{RT} (\Phi_{WE} - \Phi_{RE})} e^{-\frac{\alpha_A nF}{RT} (\Phi_e^{\Theta})} e^{-\frac{\alpha_A nF}{RT} \frac{RT}{nF} ln(c_O/c_R)} =$$

$$i_0 \left[\left(\frac{c_0}{c_R} \right)^{-\alpha_A} e^{\left(-\frac{\alpha_A nF}{RT} \Phi_e^{\Theta} \right)} \right] e^{\left(\frac{\alpha_A nF}{RT} (\Phi_{WE} - \Phi_{RE}) \right)}.$$
(82)

The corresponding relation for the cathode $(\eta < 0)$ is

$$i = -i_0 \left[\left(\frac{c_0}{c_R} \right)^{\alpha_C} e^{\left(\frac{\alpha_C n_F}{RT} \Phi_e^{\Theta} \right)} \right] e^{-\left(\frac{\alpha_A n_F}{RT} (\Phi_{WE} - \Phi_{RE}) \right)}. \tag{83}$$

We now summarise after first rewriting equations (82) and (83) using the notation Φ_{Am} and Φ_{Al} for the electrode and electrolyte potential on each side of the electric double layer at the anode and Φ_{Cm} and Φ_{Cl} at the cathode. The subscripts m and l has here the meaning metal and liquid. For convenience we further introduce the notation

$$k_a = e^{(-rac{lpha_A \, nF}{RT} \Phi_e^{\Theta})} \qquad ext{and} \qquad k_c = e^{(rac{lpha_C \, nF}{RT} \Phi_e^{\Theta})}.$$

The short-hand form of the anodic and cathodic Tafel-laws are hence formulated as

$$i = i_0 k_a \left(\frac{c_0}{c_R}\right)^{-\alpha_A} e^{\left(\frac{\alpha_A n_F}{RT} (\Phi_{Am} - \Phi_{Al})\right)}$$
(84)

$$i = i_0 k_c \left(\frac{c_0}{c_R}\right)^{-\alpha_C} e^{\left(\frac{\alpha_C n_F}{RT} (\Phi_{Cl} - \Phi_{Cm})\right)}.$$
 (85)

2. Mass Transport in the Electrolyte

The transport of species to the electrode is described by the Nernst- Plancks law

$$\mathbf{N_i} = [c_i \mathbf{u}] + [-D_i \nabla c_i] + [-\frac{z_i F D_i}{RT} c_i \nabla \Phi] \qquad (mole/m^2 s)$$
(86)

where c_i $(mole/m^3)$, z_i and D_i (m^2/s) are the concentrations, the charge numbers and the diffusivities of each specie i.

Thereupon are Φ (V) the electric potential, \mathbf{u} (m/s) the mass averaged velocity of the dilute solvent, F=96485 (C/mole) the Faraday's constant, R=8.31 (J/moleK) the gas constant and T (K) the temperature. The Nernst-Planck's law consist elementary of convection, diffusion and migration in the named order when referring to the above equation. The role of these mechanisms are discussed below and is further illustrated in figure 3.4.

Convective transport: In the bulk the mass transport is controlled by convection. A good approximation is usually that the concentration of a specie is constant in this region.

Diffusive transport: Between the viscous layer and the electric double layer, diffusion of the species are the limiting process. When the current is increased to a value for which the diffusion process no longer is fast enough, the system is running with a limiting current.

Migration: The motions of the charged species due to the electric potential field in the electrolyte.

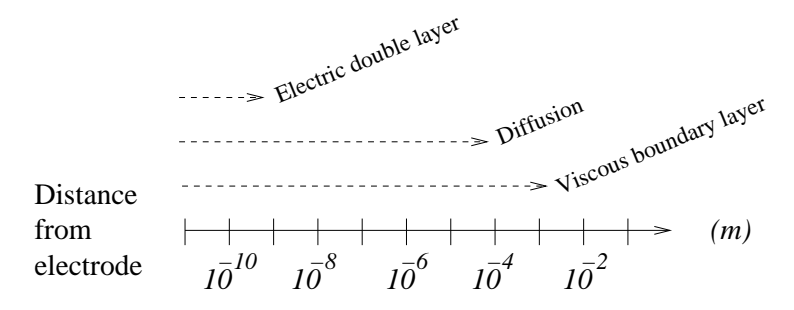


FIGURE 3.4. Current potential versus overpotential curve.

Beside the above mentioned mechanisms can, for example, also turbulent mixing or presence of gas contribute to the transport of charged ions. Dahlkild [18] introduced the mixing effects of a sheared bubble suspension according to a model for particle tracer diffusivities by Wang et al. This would add an additional term $0.12a^2\alpha^2\dot{\gamma}$ into equation (86). The definitions of a, α and $\dot{\gamma}$ are the same as in section 2, this chapter.

The electric current density caused by the total flow of electrically charged ions now writes:

$$i = \sum_{i=1}^{N} z_i F \mathbf{N}_i. \tag{87}$$

Conservation of the current

$$\nabla \cdot \mathbf{i} = 0, \tag{88}$$

and the involved ionic species

$$\nabla \cdot \mathbf{N}_i = 0 \quad \text{for} \quad i = 1, \dots N - 1, \tag{89}$$

together with the electro-neutrality condition

$$0 = \sum_{i=1}^{N} z_i c_i \tag{90}$$

finally form the governing equations of the system. The electro-neutrality condition ensures that no region of the electrolyte of macroscopic size can be electrically charged. Note that the convective term conveniently cancels in (87) due to equation (90). Also note that the coefficient

$$\sigma = \sum_{i=1}^{N} \frac{z_i^2 F^2 D_i}{RT} c_i, \tag{91}$$

which accompanies the potential gradient in the expression for current density, is the commonly known electric conductivity. This property is not constant but depends on the concentration.

Presence of gas will have effects on the conductivity as well as the diffusion. A common approach, investigated by Tobias with collaborators [50], [51] and [52] is to use the Bruggemann relation yielding

$$\sigma = \sigma_0 (1 - \alpha)^{3/2},$$

$$D_1 = D_{1,0} (1 - \alpha)^{3/2}, \quad D_2 = D_{2,0} (1 - \alpha)^{3/2}$$
(92)

where the subindice '0' indicate pure electrolyte properties.

The adjacent boundary conditions are given by the tafel laws discussed in the previous section. For gas evolving electrodes, however, the diminishment of the electrode surface area due to part wise coverage of gas, must be taken into account. The most straight forward approach is to directly reduce the active area with the void fraction at the electrode. The adequate current density at the electrode is hence

$$i = i_{ideal}(1 - \alpha) \tag{93}$$

where i_{ideal} is the current density with absence of gas ($\alpha = 0$) For a deeper and more complete insight in this matter, the reader is directed to Bockris & Reddy [8], Newman [41] and Walsh [56]. Paper 6 in this thesis involves numerical simulations based on the usage of the equations in this chapter.

CHAPTER 4

A Short Presentation of the Work

1. Computational Work

The major part of this thesis reports about numerical computations based on two-phase flow models. To be more precise, the simulations involve both the two-fluid and the mixture two-phase models, free and forced convection and finally, electrochemical mass transport equations with exponential Tafel boundary conditions. These computations are almost exclusively performed using commercial CFD or general PDE codes. In this section these codes are to be briefly presented and some numerical aspects will be discussed.

CFX

The studies reported in papers 1, 2, and 5 are made with the finite volume simulation code CFX-4.2. This is a commercial Computational Fluid Dynamic (CFD) code, trademark of AEA Technology (Harwell, UK). Both a two-fluid and a Algebraic Slip Model (ASM) are pre-installed in CFX-4.2. Also a homogeneous two-phase model as well as a Lagrangian particle tracking model are inside the CFX package. This ensures a quick start for the modelling. It is however seldom possible to do a meaningful computation without a considerable modification of attached subroutines. CFX is found to be straight-forward to use, delivering stable solutions with good convergence in a reasonable time. As the main hydrodynamic equations are pre-installed while source terms, drag terms etc. are separately implemented, it is difficult to get a clear overview of the involved equations.

Regarding the studies in this thesis, the first usage of CFX is with the two-fluid model in paper 1. The mesh of the modelled geometry, a chlorate reactor, is built in blocks which are then mounted to a unit. Different geometries are investigated and a representative mesh revealing the block structure is displayed in figure 4.1. Further numerical details of this work are discussed inside the paper.

Paper 2 and 5 involves usage of the pre-implemented algebraic slip model which fits the formulation of the mixture model and its related closure laws. In both papers the geometry is a single vertical channel.

A good resolution of the flow in paper 2 is achieved with a uniform 60x40 (width x height) mesh. Here the size of one cell represents approximately one bubble diameter.

In paper 5 a shorter but equally wide channel is resolved with a non-uniform 60x60 mesh. This finer mesh is necessary as the simulations describe a freely convected buoyant flow. It is commonly known that this type of flow easily causes bad convergence if the accuracy in the computations is low.

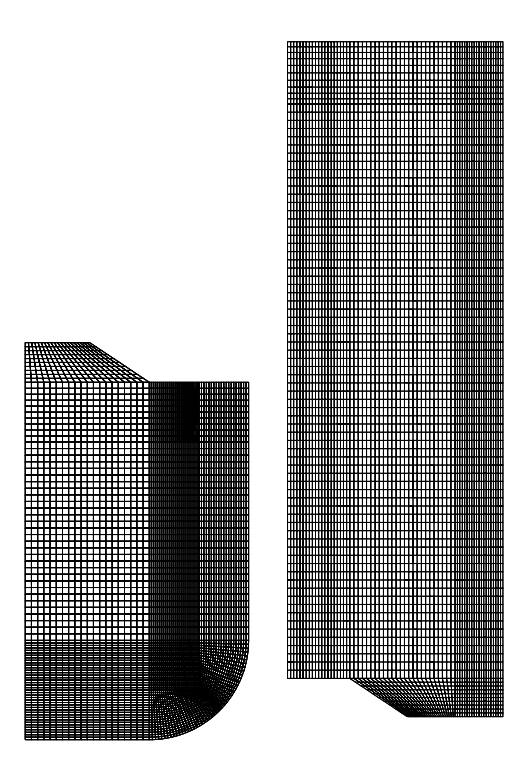


FIGURE 4.1. CFX - Block structure of mesh for a chlorate reactor. The mesh is here cut in two pieces of plotting reasons only.

FEMLAB

The fundamental difference between paper 6 and the previous papers 2 and 5 is the introduction of electrochemical transport equations and Tafel boundary conditions. These boundary conditions frequently cause convergence problems due to their exponential character. ¹ The commercial code FEMLAB (trademark COMSOL AB, Sweden) proves to be a suitable code for this type of calculations. FEMLAB is a general PDE solver based on the finite element method. Its strength lies partly in the algebraic coupling of the general equations and the boundary conditions. Although not a pure CFD code, FEMLAB has preinstalled interfaces for a direct use of the Navier Stokes equations. It is however preferable to formulate the governing equations in the general form

$$\nabla \cdot \Gamma = F. \tag{94}$$

This approach gives a very good overview of the equation system and also of the boundary conditions which are equally straight-forward formulated. Meshing,

¹In the frame of this thesis it was not possible to achieve convergence with CFX if Tafel or Butler Volmer boundary conditions were used.

implementation of mathematical expressions and choice of solver algorithm are controlled from a command-file or from a user interface.

For the channel flow in paper 6, it is necessary to resolve the thin diffusion boundary layer $((10^{-4}\ mm))$ for the ionic concentration. A dimensionless formulation of the equation system based on different length scales in lateral and vertical directions is therefore implemented in the code. With the purpose to reduce the amount of triangular cells the (width x height) 10x267 mm channel was scaled down to a dimensionless size of $1 \times 1/5$. This mesh is displayed in figure 4.2. The smallest cells which are located at the edges of the electrodes reach $10^{-9}\ m$ out from the wall.

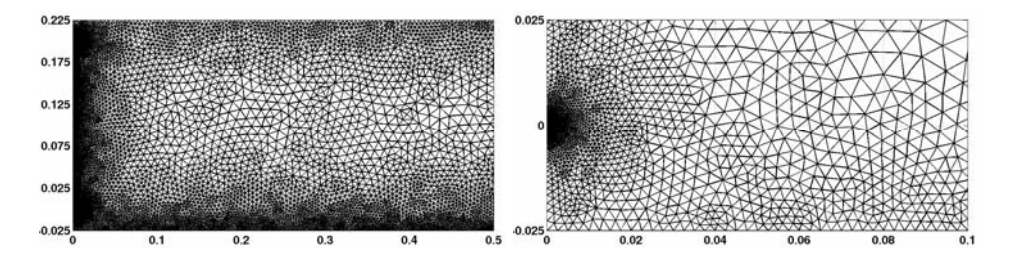


FIGURE 4.2. Triangular cells in FEMLAB mesh. Dimensions are "over-scaled" with a factor five in the vertical direction. (Left) Mesh of the half channel width. (Right) Close up around the lower left part of the geometry. Fine mesh at the leading edge of the electrode.

2. Experimental Work

All experiments are performed at Laboratoire des Écoule- ments Géophysiques et Industriels (LEGI) at INPG, Grenoble France. Although the details of each performed experiment is well described in the related papers 3 and 4, some additional comments will here follow. This section should hence be read parallel with these papers.

$Bubble\ production$

The *in-house* built Electrochemical BuBble Appliance (EBBA) consists fundamentally of a cathode- and an anode-chamber. A circular plexi glass wall separates one chamber from the other. To provide free passage for the charged ions, vertical slices are cut in the plexi glass cylinder. The cathode chamber is located as a natural part of a vertical pipe. Figure 4.3 exhibits EBBA in the lower pipe area. The pipe is directly connected to EBBA from beneath. At the upper end of EBBA a convergent diffusor is located, re-connecting EBBA with the rest of the pipe. A rectifier, supplying EBBA with current is visible to the right in the same figure. This DC supplier is able to give an output of 30 V/30 A which is sufficient for a production rate of roughly $3\ cm^3/s$ for the hydrogen gas, (see chapter 3 section 1). The flow rate of the electrolyte is indicated by the flow meter apparent to the left in the figure. The construction of EBBA is by itself a part of the work presented in paper 4, and further details on the construction is given in this paper, including a schematic drawing of EBBA.



FIGURE 4.3. The Electrochemical Bubble Appliance, EBBA, mounted in the lower part of the pipe. The flow-meter is located to the left in the picture, and the rectifier is to the right.

Optical and visual experimental techniques.

The measurements (optical fibre, laser sheet) are performed approximately 3.5 meters above the position of EBBA. To reduce optical phenomena due to differences in the refraction indexes of air and the plexi glass, the outer surface of the pipe has no curvature. A plane laser sheet, figure 4.4 indication (I), cuts vertically the middle of the pipe illuminating a rectangular area of the bubbly flow, indication (II a). The images of the laser sheet is taken with a camera pointing perpendicular to to the laser sheet and two different results can be deduced from image analysis of this illuminated sheet:

(Result 1:) The lateral void fraction distribution is assumed to be identical to the distribution of luminous points. To define the expression luminous point we first define a threshold, which is a zero level for the light intensity. Points with a light intensity brighter than this value is counted for as a bubble while less bright illuminated dots are discarded. For a constant threshold, the distribution of illuminated points is then strongly asymmetric as indicated with (III a) in figure 4.4. The number of illuminated points is hence large to the right, (where the light enters the pipe) and low to the left. It is though necessary to account for the large scatter of light. As a matter of fact, the distribution of light intensity over the diameter is roughly as schematically shown in (III b). The technique tested in this paper is to compensate this asymmetry by introducing a non-constant threshold. As a first approximation it may be assumed that the light intensity of the laser sheet decrease exponentially with the lateral coordinate. An exponential expression for a new threshold is hence fitted with least

square method to the distribution of brightness in the image. This new threshold is indicated with (III b) in the figure. Using this new exponentially decreasing threshold, a symmetric distribution of luminous points is achieved (III c).

(Result 2:) Also the bubble velocity distribution is assessed by analysis of laser sheet images. Using a long exposure time Δt with the camera, the illuminated bubbles move a distance Δl . An example is here displayed in (II b). The magnitude of the velocity is hence easily determined by $v_{bubble} = \Delta l/\Delta s$.

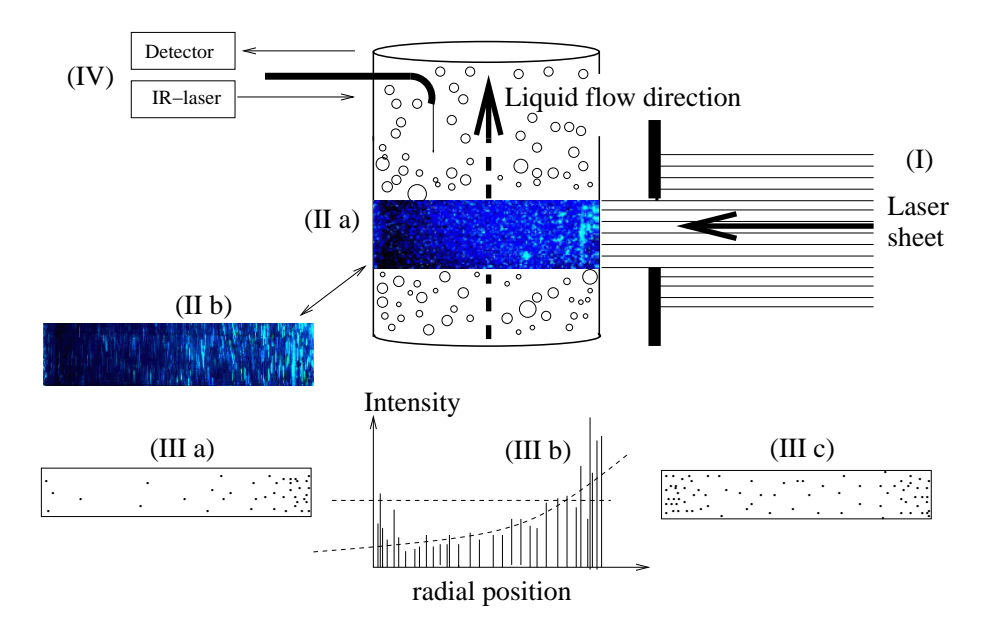


FIGURE 4.4. Experimental equipment and techniques.

A mono-modal optical fibre (IV) mounted in the flow, is pointing upstreams with the tip. The light of an IR-laser directed into the fibre, reflects on first the fibre tip, and secondly an incoming bubble. Frequency analyse of the two reflected interfering light beams leads direct to the velocity to the velocity of the bubble in the vicinity of the fibre tip. Unfortunately, the depth of detection is too low to capture the undisturbed velocity of the bubble before it start to decelerate close to the fibre.

A method is here tested which combines analytical and numerical ingredients, describing this deceleration, with the measured data in order to determine the undisturbed velocity. This is performed by means of a matching procedure, in which the free stream liquid velocity and the radius of the bubble are unknown parameters to find. As a matter of fact, each combination of bubble radius and free stream velocity appears to form a unique deceleration. An example of this matching procedure is given in figure 4.5. The rather high sensitivity of the procedure is apparent and a proper combination of radius and velocity is found after only a few tries. This method requires however a precise analytical/numerical description of the approach of the bubble. The method proves to predict reasonable velocities but it overestimate the bubble radius, compared to the average

bubble radius of the mixture. Alternatively it might be suggested that the optic fibre in a selective way only detects large bubbles.

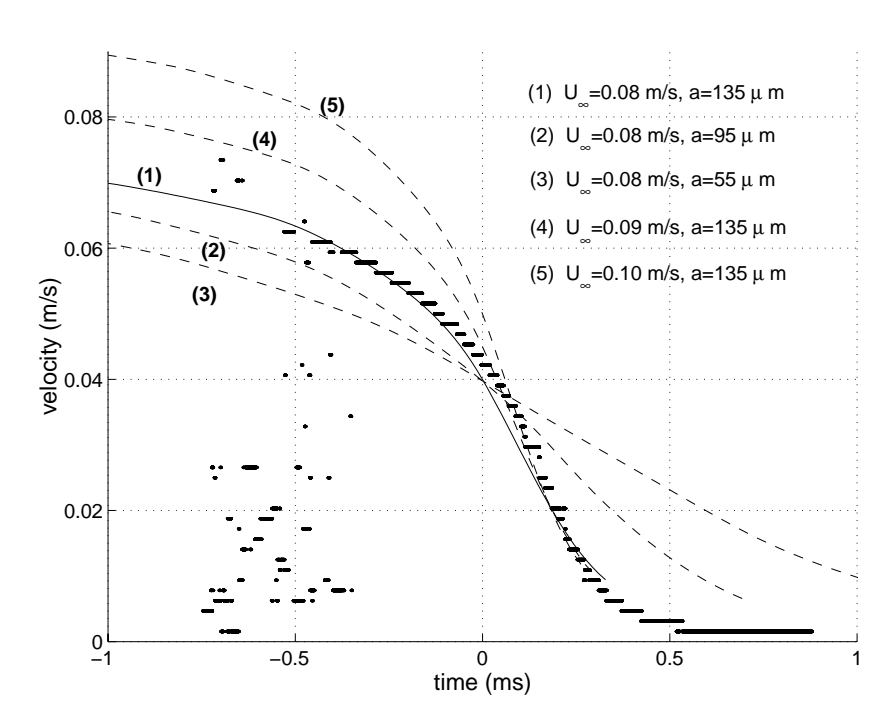


FIGURE 4.5. Matching of the velocity achieved with analytical relations with the measured optic fibre velocity.

3. The Papers

3.1. Paper 1.

The internal two-phase flow in a conceptual chlorate reactor, figure 4.6 is investigated by means of numerical simulations. The aim of the study is to identify geometrical factors and features in the flow, which are important to consider from a designing point of view. The modelled reactor consists of a stack of flat electrodes, vertically placed face to face and separated by a narrow channel filled with electrolyte, in the bottom of a large tank. As voltage is applied, an electric current runs through the stack and hydrogen gas is evolved at the cathodes. The bubbly electrolyte mixture is continuously forced up through the channel as an effect of buoyancy induced circulation. The simulations, performed with the commercial code CFX (Harwell, UK), are based on a two fluid model using an interface drag in the Stokes regime. The gas phase is introduced along the top of the stack and evacuated at the top surface by use of source terms. The flow in the stack itself, is modelled by considering the stack to be a porous media with internal parallel flow.

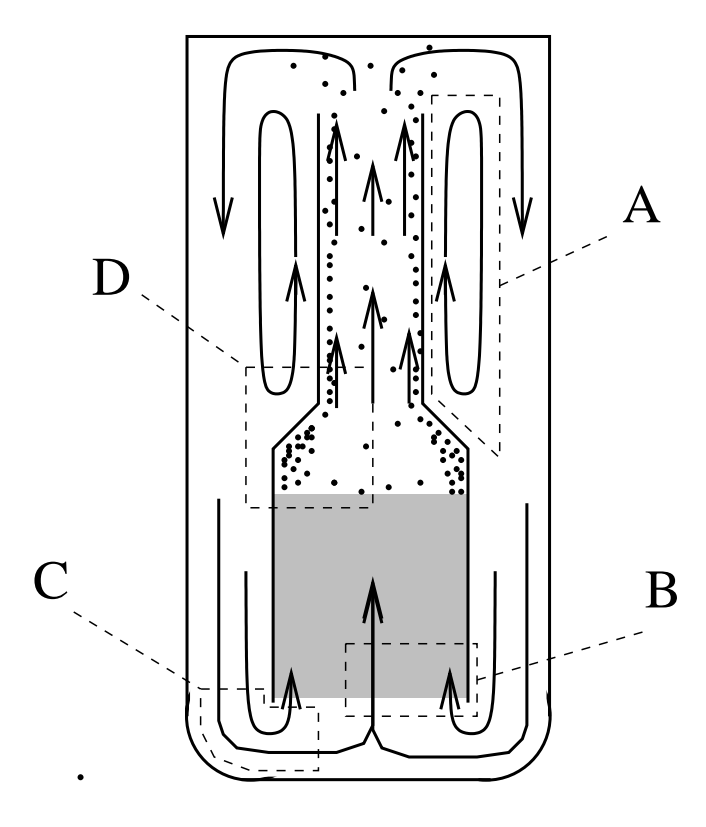


Figure 4.6. Schematic picture of a gas-lift chlorate reactor.

Two domains with different flow characters can be identified in the reactor:

(Domain 1) The reactor tank outside the electrode stack, where the buoyant rise of the individual bubbles induce circulation of the electrolyte due to the gas/liquid interface drag. A chimney is placed over the stack in order to control the direction of the flow and to promote the magnitude of the circulation.

(*Domain 2*) The electrode channels, where the convection is mainly forced due to the flow outside the stack. It is though demonstrated in paper 2 that local buoyancy however also affects the flow inside the narrow channel.

Some distinctive features of the flow:

(1) As the flow exits the top of the chimney and is directed downwards, a stagnant zone (indicated with (A) in figure 4.6) develops along the outer wall of the chimney. Whereas a full control over the circulation is beneficial, this zone should be removed. A possible method is to re-design the outside wall of the reactor by introduction of a long baffle, effectively guiding the flow downwards, parallel to the chimney.

- (2) In the bottom of the tank, the electrolyte enters the stack, (area (B) in figure 4.6, with a strongly non-uniform profile. As mass transport in the electrolyte channel is promoted by the electrolyte flux, this is highly unfavourable. It is demonstrated in the study that installation of baffles in area (C) has only a minor influence on the entering profile of the velocity. On the other hand, a simple and effective method to cause the electrolyte to enter the stack uniformly, is to prolong the vertical distance between the bottom of the tank and the stack. This method proves effective also for increasing the *total* flow rate through the cell.
- (3) As the production of hydrogen gas is assumed equal in all electrode channels, the low velocity in an electrode channel leads to high void fraction. Consequently the void fraction is higher closer to the stack walls where the electrolyte flux is low. Along the lower inside of the chimney, (area (D) in figure 4.6, a zone with high concentration of gas hence appear. This "bubbly layer" persists along the length of the chimney and causes the electrolyte to flow with higher velocity close to the walls of the chimney.
- (4) The effects of scale-up are investigated and it is clear from the results that it is beneficial to increase the size of the reactor since the total flow rate thereby is enhanced.
- (5) Another method to increase the total flow rate through the cell is to apply a higher cell voltage and thereby increase the gas production. The relation between gas production and total cell flow rate is investigated and demonstrated in figure 4.7. Further is a complementary 1D model developed which is able to predict this relation.

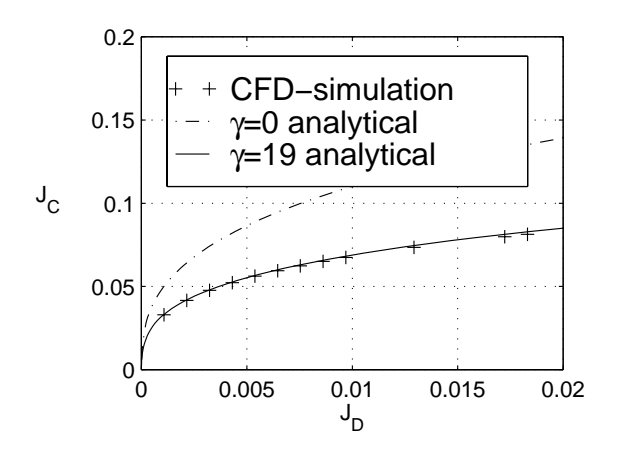


FIGURE 4.7. Average superficial velocities J_D and J_C (m/s) for dispersed and continuous phase in the chimney. The parameter γ is an unknown loss coefficient for the 1D model which has to be determined by matching.

3.2. Paper 2.

The developing two phase channel flow in a gas-evolving electrolytic cell is investigated numerically. The measurements of the narrow channel are chosen in purpose to capture the flow inside the electrode stack which is previously discussed in paper 1. This paper can hence be considered to be a detached continuation of that study. A hydrodynamical drift flux two-phase model as described by Ishii [29] is used with complementary empirical laws describing the motions of the the gas phase relative to the mixture. These empirical relations are originally developed for shear induced hydrodynamical diffusion and migration of particles. It appears that this approach proves to give qualitatively good results.

In this work, parameter studies are performed with respect to for example the bubble radius, the rate of gas production and the inlet velocity of the electrolyte.

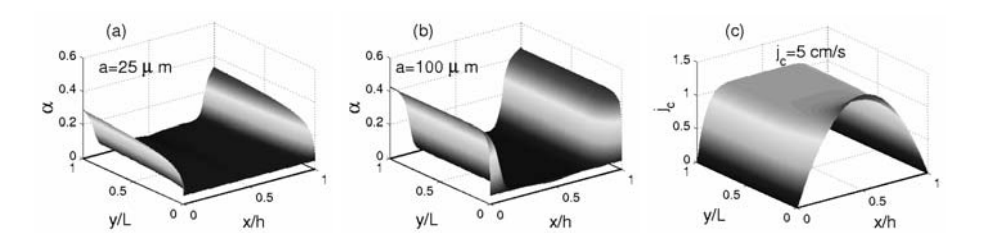


FIGURE 4.8. The development of bubbly layers along the walls of a 0.4 meter long channel. Bubble radius a, superficial electrolyte velocity j_c At the entrance of the channel the velocity distribution is parabolic and the averaged void fraction is 5 %. (a) Developing bubbly layer, $a=25~\mu m$ and $j_c=1~m/s$. (b) Established bubbly layer, $a=100~\mu m$ and $j_c=1~m/s$. (c) Typically flattened velocity profile, $a=25~\mu m$ and $j_c=0.06~m/s$.

Some selected results are worth being mentioned:

- (1) Although most computations are made with evolution of gas at one wall, a test case with pure transport of gas at a total void fraction of ~ 5 % and a velocity of 1 m/s, is investigated. In qualitative agreement with existing literature, for example [5], [44], [46], bubbles relocate from a homogeneous distribution to dense bubbly layers along the walls. For a parabolic velocity profile at the entrance, this process is here exhibited in figure 4.8a,b. As discussed in the paper, the establishment of the developed bubbly layer is slower for smaller bubbles. A certain flattening of the velocity profile is almost always present (figure 4.8c). For higher liquid flow rates, the visible buoyancy effects on the velocity distribution are small but not negligible. In the mathematical modelling, the flux towards the wall is caused by the Saffman force [47].
- (2) It appears that the size of the bubbles are directly responsible for the character of the bubbly layer. Larger bubbles form a thicker and less concentrated bubble layer than bubbles of smaller radius. Figure 4.9 illustrates this feature which is in line with the modelled transport mechanism related to mutual bubble interactions.

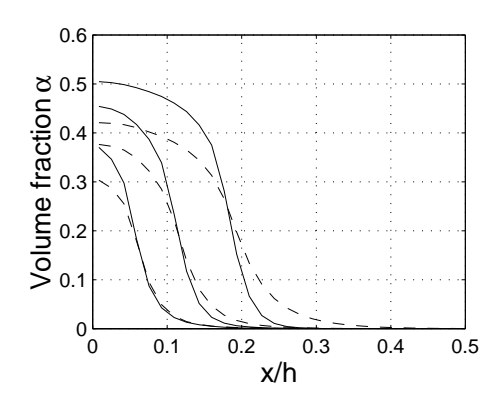


FIGURE 4.9. A developing bubbly layer adjacent to a gas evolving electrode. at 15, 45 and 125 channel-widths downstream (bubble radius $a=25~\mu m$, solid line, bubble radius $a=100~\mu m$, dashed line). The superficial velocity is in both cases $j_c=0.6~m/s$

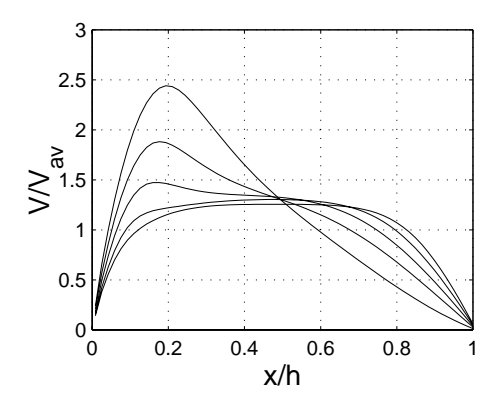


FIGURE 4.10. The shifting of velocity maximum towards the gas evolving wall for a low liquid flow rate compared to the gas flow rate.

(3) As the ratio between the gas flow rate and the total gas/liquid flow rate is increased, 2 the buoyant effect on the velocity distribution is obvious. Here illustrated in figure 4.10 A shifting of flow towards the gas evolving wall take place. It is expected (although not demonstrated in this paper) that for considerably high values of β a counterflow at the opposite wall can appear.

3.3. Paper 3.

In this work, the ability is investigated of using a mono-modal optical fibre to measure the velocity of moving gas-liquid interfaces such as slugs or micro-bubbles. Such a measurement technique could be useful inside concentrated

 $^{^2}$ This ratio is denoted β and defined by equation (14).

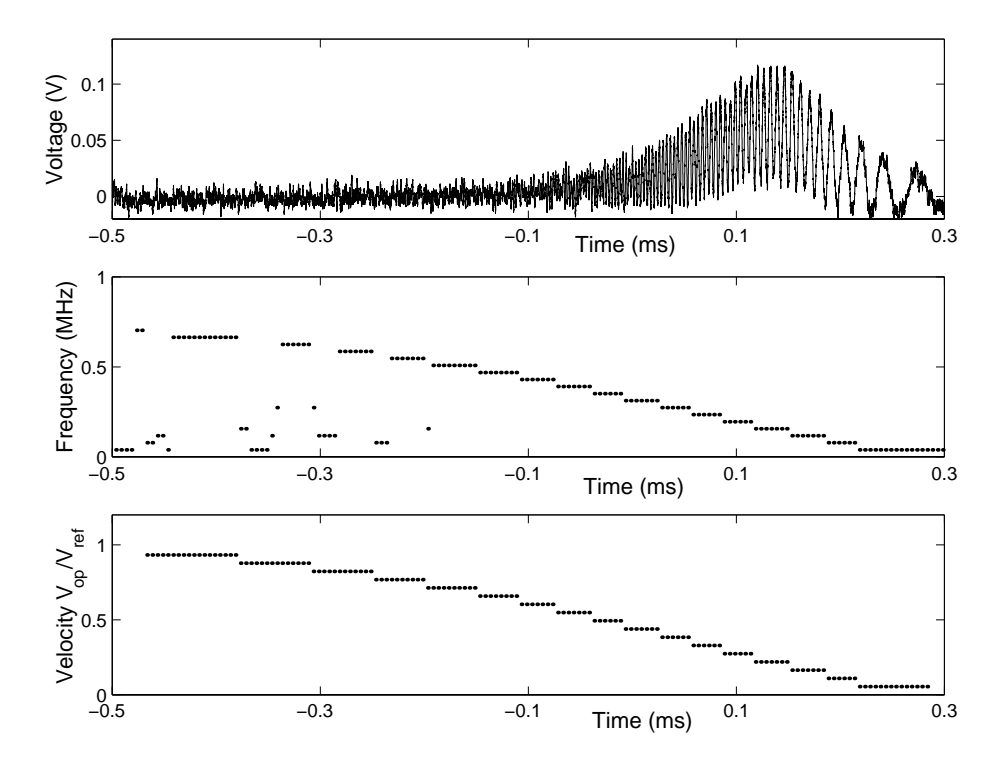


FIGURE 4.11. Processing of the interference signal from detection of a bubble. (a) The signal of an approaching bubble, acquired by the acquisition system. (b) FFT/sliding window analysis of the signal. (c) Noise is removed from the spectral content, the subsequent frequency is transformed to the velocity V_{op} and scaled with a reference velocity V_{ref} .

two-phase mixtures where ordinary LDA measurement is difficult to perform due to the high interfacial area density.

An IR laser beam is directed into a cleaved optical fibre which in its turn is directed upstream towards an arriving gas bubble, slug or front. As the light is reflected both at the tip of the optical fibre and at the incoming gas-liquid interface outside the fibre, the velocity of the approaching interface can be estimated by analysing the interference pattern between the two reflected light beams. A typical interference pattern received by the acquisition system and its interpretation to the approach velocity are illustrated in figure 4.11.

Experiments have been performed with flat fronts, slugs and micro-bubbles approaching a downwards-pointing optical fibre. For flat fronts and slugs in constant motion, it was found that the velocity of the approaching interfaces can be measured with an acceptable precision.

Continuous experiments were also carried out with electrochemically produced micro-bubbles. For these bubbles it was not possible to directly asses the undisturbed velocity upstream of the fibre. This is partly explained with a insufficient depth of detection. Another explanation could be a weak reflection at the

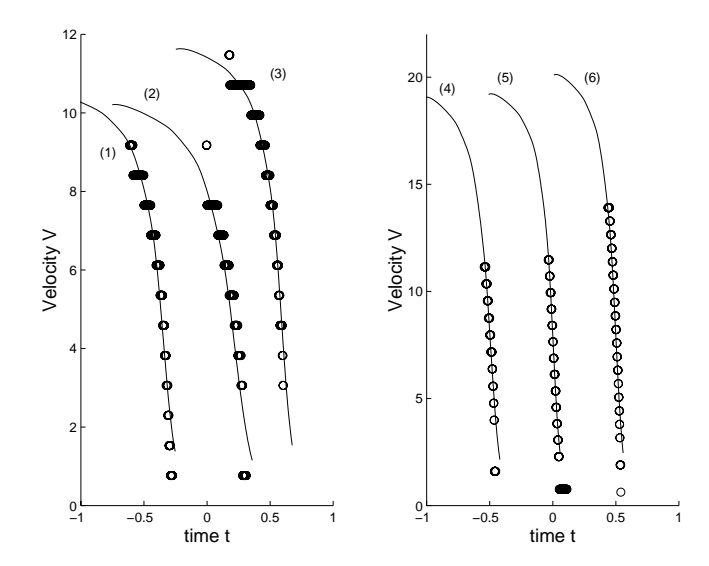


FIGURE 4.12. Adaptation of optical signals for micro bubbles with analytical prediction. Velocities from optical signals (dots) and from semi-analytical prediction (solid); dimensionless time. (left) The curves (1)-(3) displays three signals for pipe Reynolds numbers $Re_H = 925$, 970 and 1120. (right) The curves (4)-(6) displays three signals with $Re_H = 2160, 2300$ and 2350.

surface of the bubbles. With the aim to compensate the measuring technique for this shortness, a method of extrapolation based on analytical developments is investigated and proposed. This method is inspired from an analytical/numerical work performed by Dagan et al. [16], devoted to the creeping approach of a spherical particle at the vicinity of a flat disk. After combination of these theoretical ingredients with a time-frequency analysis of our optical signals, it is possible to infer both the bubble size and the undisturbed velocity.

Some highlighted results:

- (1) Hydrogen bubbles are electrochemically produced at a cathode surface a short distance upstream of the optical fibre. Special attention is devoted to the separation of hydrogen bubbles from the oxygen bubbles evolved at the anode in the meantime. A mixing of the two gas phases can potentially cause explosion. The size of the hydrogen bubbles, estimated with a visualisation technique, is found to be a $\sim 110 \pm 40~\mu m$.
- (2) The optical fibre is used for measurements of (i) vertically approaching gas slugs and (ii) vertically incoming liquid surfaces (fronts). These measurements are performed with the aim to test the performance of the technique. Reference velocities are provided by traditional conventional methods. ³ It appears from these measurements that the optical fibre is able to capture a correct

 $^{^3}$ An automatic laser/photo-detection technique is used on the slugs while the liquid surface velocity is measured with a visual method.

velocity with an uncertainty of $\approx 15\%$. The depth of detection is measured to be $\sim 300 \ \mu m$, i.e roughly 1.5 bubble diameter.

- (3) The velocity of rising hydrogen bubbles in upward channel flow is measured with the optical fibre. The undisturbed velocity of the bubbles is assessed by matching of the measured velocity in vicinity of the fibre tip with an analytically predicted velocity decrease close to the fibre. This method allows to determine both the bubble velocity and the bubble size. Some examples from this matching is exhibited in figure 4.12 Apparently, the results confirm that this technique allows to measure a relevant bubble velocity. On the other hand, the technique deliver bubble sizes which are much larger than what is measured with a conventional visual method. This could suggest that the fibre is "selective" in that way that only larger bubbles give sufficiently strong light reflections.
- (4) As a curiosity, signals are captured possibly arising from bubbles bouncing at the tip of the fibre.

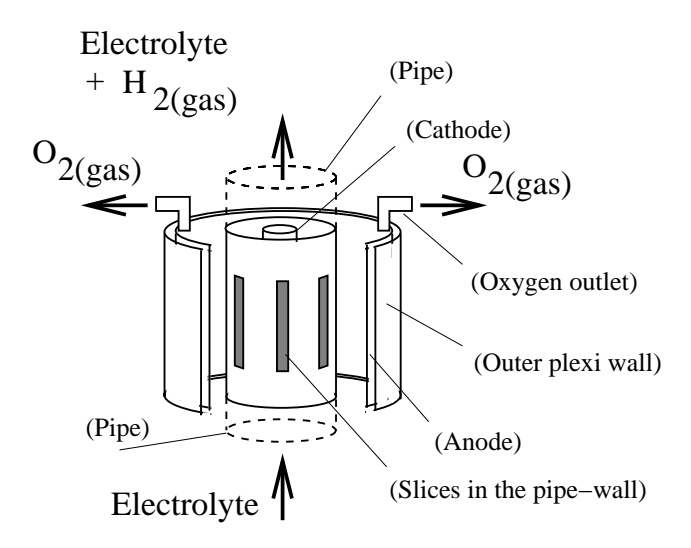


FIGURE 4.13. The Electrochemical Bubble Appliance, EBBA.

3.4. Paper 4.

A special Electrochemical Bubble Appliance (EBBA), figure 4.13, is constructed for the purpose of producing micro-bubbles. The device is mounted in the lower part of a 5 meter high vertical pipe system which is filled with a Sodium sulphate solution. Due to the high interfacial ratio for a non-dilute suspension of micro-bubbles, conventional measuring techniques often fails. Considerable efforts are therefore spent on the design of the experimental facility and on the development of adapted measuring techniques, including the associated data processing.

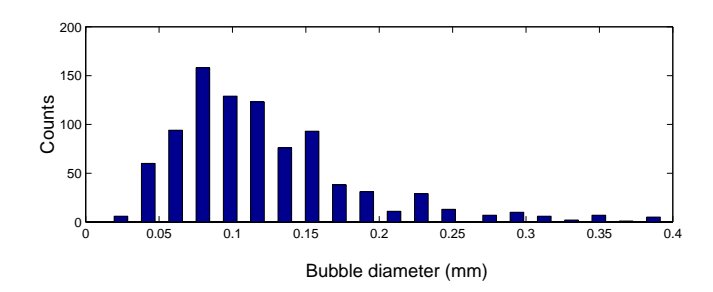


FIGURE 4.14. Size distribution of H_2 bubbles.

- (i) The hydrogen producing cathode should be mounted in the upward pipe flow in such way that the liquid shear rate is as uniformly distributed as possible over its surface. The cathode surface must be smooth and the area should be maximised, but with a minimal presence of edges and corners. Any deviation from these points directly cause larger and less mono-dispersed bubbles.
- (ii) A free passage for electrically charged ions must be ensured, but without violating the separation of the hydrogen gas evolved at the cathode from the oxygen which is evolved at the anode. Mixing of the two gases can cause explosion.

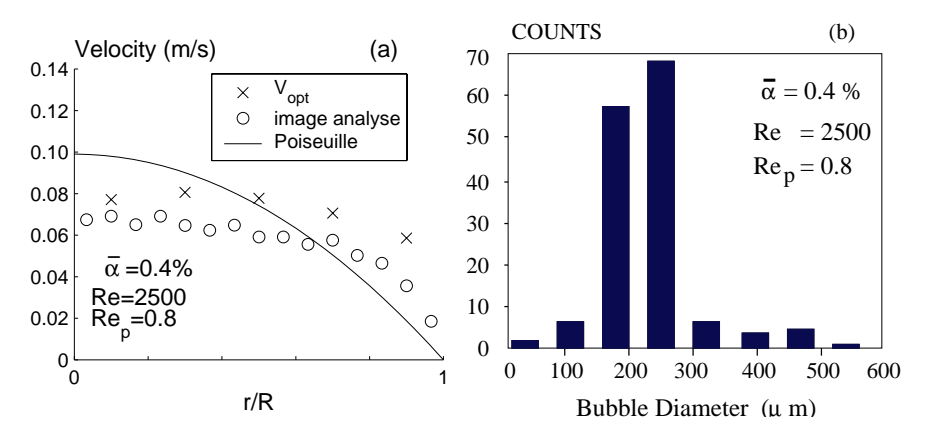


FIGURE 4.15. Experimental data for Re = 2500 and I = 5A, measured with the mono-modal fibre-optics velocimeter. (a) Velocity profile for the detected bubbles. (b) Size distribution derived from the matching procedure (paper 3).

Measurements are performed on liquid flow rate, gas and liquid velocity distribution, gas hold up and the void distribution. The liquid flow rate is roughly indicated by a flow meter connected to the pipe, while the bubble velocity distribution is measured with a visual technique using long time exposure pictures.

The distribution of the liquid velocity is assumed to follow the distribution of the gas velocity, but with a presumed relative velocity effectively subtracted. A complementary investigation of the gas phase velocity distribution is performed by means of an optic fibre velocimeter previously discussed in paper 3. A two-valve construction gives access to the gas hold up with good precision. Studies on the void distribution is based on visualisation using a laser sheet.

This last technique is not completely straightforward since the strong scatter of light in the measuring zone necessarily must be compensated for.

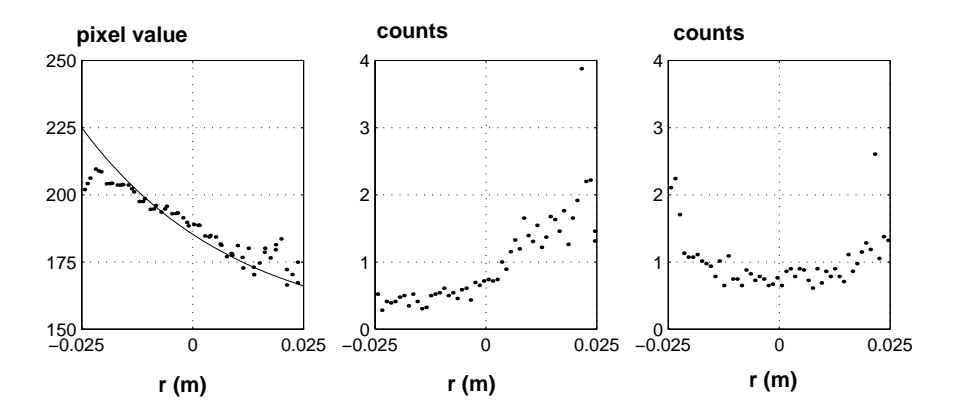


FIGURE 4.16. (a) Grey level values distribution as directly calculated from the video-inverted image. The solid line is an exponential fit. (b) Normalised counts of the luminous points due to light reflections from the micro-bubbles as deduced from the original image. (c) Same as figure b after removing the mean grey value.

Some selected results.

- (1) The electrochemical bubble appliance (EBBA), figure 4.13, is a well working device, generating microbubbles with acceptable deviation in size.
- (2) The hydrogen bubble size is determined visually. The radius, $a=100\pm 50~\mu m$ (figure 4.14) is affirmative to a previous investigation in paper 3.
- (3) It was not possible to assess the hydrogen gas flow rate directly via Faradays law. In fact, the observed efficiency in producing hydrogen gas was roughly 65%. Possible explanations are dissolution of hydrogen gas into the electrolyte and bubbles escaping into the anode chamber.
- (4) Fibre optical measurements of the gas velocity distribution and the bubble size supports a previous result (paper 3) that the technique is somewhat selective smaller bubbles do not seem to give rise to the same amount of acquisitioned signals. This is illustrated in figure 4.15.
- (5) A method is tested for compensating the strong light scatter in the images of the laser sheet. As demonstrated in figure 4.16, strong scatter of light

give rise to a non-symmetric distribution of luminous points on images of the laser sheet. Subtraction of the mean grey level appears to be a possible method to assess the symmetric distribution of the bubbles.

(6) The physical results are of somewhat qualitative nature. The typical trend in upward bubbly pipe flow, with void fraction peaks near the walls is recovered. Somewhat peculiar is the thickness of this bubbly layer (here $\sim R_{pipe}/6 \approx 40$ bubble diameters). Possibly the flow was not fully developed despite the long distance (> 150 R_{pipe}) from the inlet of the pipe.

3.5. Paper 5.

Freely convected two phase flow in a narrow and short vertical electrode channel (3 mm x 120 mm) is investigated numerically. The dimensions of the channel are the same as in the experiments by Boissonneau & Byrne [6]. The free convection is induced by the interface drag from rising buoyant microbubbles, evolved at the cathode covering the mid-third of the channel height. The hydrodynamical two-phase drift flux model introduced in paper 2 is used for the numerical simulations.

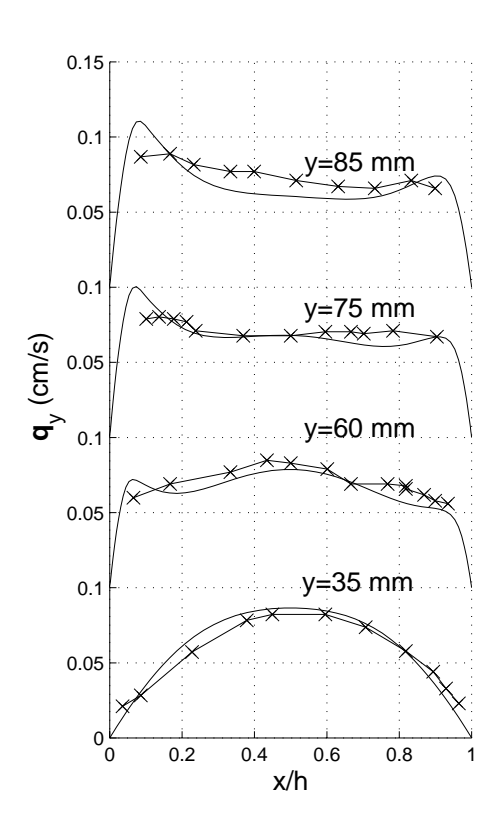


FIGURE 4.17. Electrolyte velocity profiles. Hydrogen is evolved at the cathode (x=0) and Oxygen at the anode (x=1). Experimental data by Boissonneau & Byrne[$\mathbf{6}$] (x), and present model (solid line).

Parameter studies are performed with respect to bubble size, gas production and channel width. As expected, a higher gas production resulted also in an increased liquid flow-rate.

Finally, comparisons are made to data measured by Boissonneau & Byrne for evolution of gas at both anode and cathode.

Some results in highlight

- (1) It is demonstrated that larger bubbles dramatically increases the flow rate of electrolyte. The main reason is likely that larger bubbles form a thicker bubble plume (as discussed in paper 2).
- (2) For certain channel widths, an inflow of electrolyte is observed over part of the channel exit, consequently reducing the net flow rate.
- (3) Simulation results were compared to measurements by Boissonneau & Byrne [6], on a cell with double-sided gas production. The electrolyte velocity profile agreed considerably well in the part of the channel where the flow was laminar, figure 4.17.

3.6. Paper 6.

A gas evolving electrochemical cell is investigated from both an electrochemical and hydrodynamical point of view. The two phase drift flux model previously tested in paper 2 and 5 is implemented together with conventional relations for transport of charged ions. The electric potential field, the current density and the distribution of ion concentration is modelled using non-linear boundary conditions based on Tafel laws. Numerical simulations are performed on a slender and long (10 mm x 267 mm) vertical gas evolving anode/cathode channel. Figure 4.18 illustrates the principal design of the channel. No gas is evolved in the insulated inlet and outlet sections of the channel. The electrolyte which is convected through the channel with force, is entering the channel with a parabolic velocity distribution. As buoyancy effects gradually are strengthened along the channel, a lateral shifting of the velocity profile takes place. Velocity peaks form in the vicinity of the gas evolving walls. This feature is directly dependent on the rate of gas evolution. A stronger velocity peak is consequently formed close to the cathode where hydrogen is evolved with the double rate compared to the rate of oxygen at the anode, (see figure 4.18).

Regarding the transport of charged ions, this is a process controlled by convection, migration and diffusion. The consumption of hydroxide ions along the anode, together with a diminishing conductivity due to a higher gas void fraction in the upper part of the channel, give rise to a non-uniform current density distribution along the electrodes. The difference in current density between the upper and lower part of the electrodes is found to be considerable, although not as large as reported earlier from Hine & Murakami [26] and Dahlkild [18]. Further, it is found that the current density strongly peaks at the ends of the electrodes. These end effects are well known features in the electrochemical literature and are here studied from first principles of two-phase fluid dynamics in combination with laws from electrochemistry. Simulations are also performed without the inert inlet and outlet sections. Large differences between these two cases was found in the distribution of current density as well as the void fraction and the ionic concentrations along the electrodes. The total current integrated over the

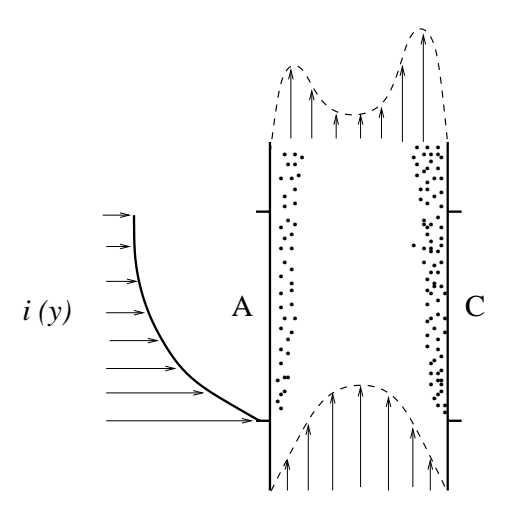


FIGURE 4.18. The non-uniform current density along the electrode channel which starts and ends with inert walls. Higher gas evolution at the cathode to the right.

cell however did not differ with the same magnitude. Some examples of current distribution from this study, measured data of Hine & Murakami, as well as a qualitative similar chlorate cell investigated by Byrne et al. [11] are displayed in figure 4.19. In conclusion, the present modelling technique is a promising tool for future detailed studies of gas evolving electrochemical cells.

Some highlighted results

- (1) It is in the study demonstrated that the current density distribution is more non-uniform for higher cell-voltages.
- (2) A large current peak appears at the edges of the electrodes. These end effects do not appear if the electrode cover the full length of the computation domain. It is therefore necessary to model also the geometry around the edges of the electrode. The performed simulations indicate that distribution of ion concentration as well as void fraction and thereby the current density distribution differs considerably between studies with and without consideration of the regions up- and downstream of the electrode edges .
- (4) The Tafel boundary conditions requires a computational solver with high accuracy. The commercial code FEMLAB used for the performed computations is found to be stable and appropriate for this purpose.
- (5) Due to a locally strong end current, a relatively high void fraction forms directly at the lower end of the electrode. Along the remaining length of the electrode the void is then only slightly increased. As it is assumed that coverage of gas reduces the effective electrode area, this would indicate that the effective electrode area fraction is rather constant over the electrode.

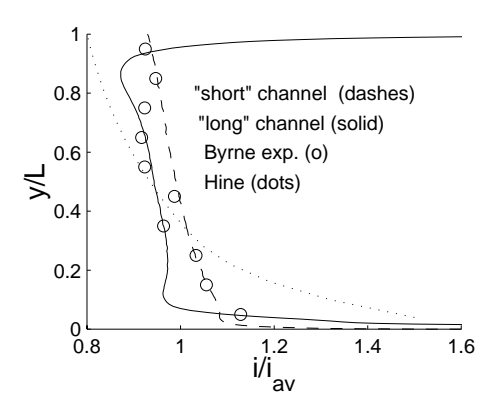


FIGURE 4.19. Current distribution along the anode. Experimental data by Hine (solid line). Experimental data by Byrne et al. (o). Present model in *long* channel (dashed-dotted line), and *short* channel (dotted line).

CHAPTER 5

Outlook

One of the aims with this thesis is to point out possible directions for further studies in the field of electrochemical gas-evolving cells and reactors. Regarding the numerical work, a continuous supply of faster computers provide the engineers with better and faster hardware tools for the design and construction of reactors. On the other hand, the same engineers must be provided with appropriate software tools, such as for example mathematical and models and numerical codes. If now this thesis is one step in this process, the possible extensions are many. In this chapter, some suggestions will be given of how the work in this thesis can be continued. Also a brief discussion about design methodology for the next generation of gas-evolving electrochemical reactors will follow.

1. Improvements of the Techniques, Tools and Models

The mathematical modelling involved in this thesis can be further developed. In the two-fluid model as well as in the drift flux model should the turbulent mixing of gas phase be considered. This would affect the distribution of bubbles and thereby the buoyancy driven flow, both in the macro-scale circulation in the reactor and in the electrode channel. The lateral lift forces on the bubbles should be accounted for and introduced additional to the drag term in the closure laws of the two-fluid model. Some sort of hindering velocity function could with advantage also be added to the two-fluid model.

A validation must be made for the detailed closure terms used in the drift flux model. This includes a careful investigation of the near wall region. Indeed, it is of high importance to model the near-wall region correctly whereas the current distribution along the electrode depends strongly on the mass transport in this region.

An exiting continuation of paper 6 is to do a more complete implementation of an electrochemical process, e.g. the chlorate process. This would imply a simultaneous simulation of non-uniform gas evolution fully coupled to the transport of 5-10 ionic species. This type of numerical tool would indeed be powerful in the design process of electrodes and the adjacent geometry.

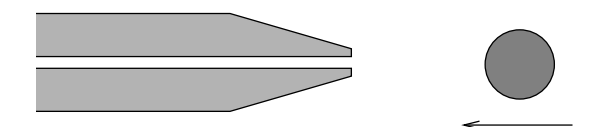


FIGURE 5.1. An optical fibre with a sharpened tip.

5. OUTLOOK

Regarding the performed experiments, several things can be mentioned.

The fibre optics velocimeter is a promising tool for measurements of bubble velocity as well as bubble size, but the technique is still in need of improvements. Apparently, the fibre is somewhat selective and discriminate smaller bubbles. A possible way to avoid this unwanted behaviour could be to sharpen the tip of the fibre, figure 5.1. This should increase the relative size of the bubble and thereby simplify for the bubble to come close to the core of the fibre. In complement to this equipment improvement, the semi-analytical model, here based on a work by Dagan, which is used in the matching procedure must be further developed. A more realistic bubble dynamics has to be considered, by introducing notably the added mass. Also the possibility to fully replace the semi-analytical model with a data-base built from numerical transient simulations of bubble / fibre-tip interactions, can be investigated.

The bubble generating electrochemical device EBBA proves useful for the production of tiny hydrogen bubbles. A few improvements are though necessary. It is unclear why the measured gas production deviated roughly 35 % from the expected production rate. If the explanation is that the hydrogen gas is dissolved into the electrolyte, the rate of this process must be investigated. If, on the other hand, the hydrogen bubbles simply escape into the anode chamber, the opening between the anode and the cathode chamber must be modified.

The vertical pipe above EBBA can very well be replaced with a longer and more narrow tube. This would reduce the inlet length for a fully developed flow. A higher liquid velocity would then be possible without transition to turbulent flow

Further validations must be performed on the image analyse technique here developed in order to compensate for the large scatter of light.

2. A New Generation of Electrochemical Reactors

The large majority of electrochemical reactors and processes of today are designed with empirical techniques. Most often with consideration of only basic hydrodynamical aspects, and with no optimisation of the flow features. In some more or less successful cases the outcome is a reactor which effectively take into account the presence of gas. The bubbles are here transported away from the electrodes and the main circulation of electrolyte in the reactor is induced by the buoyancy effects. One example here is the gas-lift chlorate reactor discussed in paper 1. Still, minor modifications motivated by modern two-phase numerical modelling, are often enough to considerably improve both the quantity and the quality of the circulation.

In worst cases, no account at all are taken to the evolution of gas. Flat horizontal electrodes found in chryolite baths with electrolysis of aluminium could be an example. Instead of promoting an effective beneficial transport process away from the electrode surface, the evolved bubbles form a dense layer under the electrode in top. A direct consequence is then a deteriorated mixture conductivity and a reduced area of active electrode. The motions of a single bubble in this bubbly film are unknown, but it might be assumed that the motions of the film itself in the lack of dominating flow directions are chaotic and sensitive for small disturbances. Possibly might stagnant zones with a minimum of inflow of fresh electrolyte establish. To conclude, the external control of the flow patterns are often minimal. In some cases reactors based on flat horizontal electrodes could

be improved by the superpose of an externally controlled main flow, but in others the benefits of a total re-design would be larger.

Improvements of existing reactors could for example involve the addition of a chimney over an electrode package, or prolongation of an already present chimney. The bottom of the reactor can be extended in order to promote a more uniform velocity distribution in the electrode package. Stagnant zones in the reactor can be discovered by numerical two-phase simulations of the internal circulation, and then possibly be removed by the mounting of baffles. In conclusion, a numerical analyse of the internal two-phase flow can most likely suggest considerable performable improvements for existing reactors.

The design process for a new reactor is never straightforward. It is a complex and iterative procedure where electro-, thermo- and hydrodynamical aspects must be considered simultaneously. It is further necessary to optimise the energy consumption against the production-rate. Last but not least, the reactor must be possible to build at a reasonable price.

In conclusion: referring to the present thesis, especially paper 1 and 6, it is obvious that with the existing numerical two-phase flows tools of today, a consideration of the two-phase flow stands as one of the central points in the design process of the next generation of gas-evolving electrochemical reactors.

Acknowledgments

During the years I was working on this thesis, I was fortunate to be constantly surrounded by colleagues who provided an stimulating atmosphere.

First of all I would like to thank my advisor and friend Anders Dahlkild. Without his deep knowledge, enthusiasm and guidance in the subject of fluid dynamics and two-phase flows, I would still be trying to converge my very first simulation. He has always been patient with me and given me the time when I needed it.

Fritz Bark is acknowledged for his work within the FaxénLaboratory. The amount of work he has devoted to this project is enormous. My stay at Laboratoire des Ecoulements Géophysiques et Industriels (LEGI) at INPG in Grenoble is one of the best periods of my life. Not only for the skiing but for the chance to encounter the world of experiments. I really learned a lot during these months. Many thanks to Laurent Davoust and Alain Cartellier for sharing their large experimental skills with me. The foundations "Erik Petersohns minne" and "Alice and Knut Wallenbergs stiftelse" are acknowledged for economical support of my stay in France.

I appreciate the help I have achieved from persons at the electrochemical department. Thanks to Mårten Behm, Göran Lindberg and especially Phil Byrne who also helped me to build EBBA and to get started in France.

Thanks to my room-mates during the years for many enjoyable discussions not only concerning fluid-dynamics. In particular Jan, Casper, Sima and Jerome have always helped me to keep my good mood up.

My largest gratitude to Ed Fontes who taught me about chlorate reactors, pushed me forward in my work, and helped me to start my computations in Femlab. I highly appreciate your believe in me.

Merci aux techniciens Laurent et Jean-Marc pour toute l'assistance dans le lab. Les Amis grenoblois Nico, Flo, Berangere, Vero, Benoit, Paulo et les autres pour les fetes, les beaux jours dans les alpes et la voile sur la cote d'Azur. Je n'oublierai jamais le temps passé là-bas.

I would like to thank my whole family, for providing solid roots in my life. Finally, I want to send my love to my wife Evy Gunn who supported me during hard days of weak motivation - *Elsker deg*.

Bibliography

- [1] Acheson D.J. Elementary Fluid Dynamics. 1990. Oxford applied mathematics and computing science series. Clarendon Press, Oxford.
- [2] Modern compressible flow with historical perspective, Second edition. Anderson J.D. 1990.McGraw-Hill International Editions. Aerospace series.
- [3] Auton T.R., Hunt J.C.R., Prud'Homme M. The force exerted on a body in inviscid unsteady non-uniform rotational flow. J. Fluid Mech. 1988, 197, pp. 197-241.
- [4] Bankoff S.G. ASME, J. Heat Transfer 82, 1960 p.265.
- [5] Beyerlein S.W., Cossmann R.K., Richter H.J. Prediction of bubble concentration profiles in vertical turbulent two-phase flow. *Int. J. Multiphase flow*, (1985), **11:5**, pp 629-641.
- [6] Boissonneau P. and Byrne P. An experimental investigation of hydrogen gas bubble-induced free convection in a small electrochemical cell. J. Appl. Electrochem. 2000, 30, 767
- [7] Bockris J.O'M. Reddy A.K.N. 1977. In modern electrochemistry, Vol. 1, Plenum.
- [8] Bockris J.O'M. Reddy A.K.N. 1977. In modern electrochemistry, Vol. 2, Plenum.
- [9] Byrne P., Simonsson D., Lucor D., Fontes E. A model of the anode from the chlorate cell. Fluid mechanics and its applications, 51 Transfer phenomena in magnetohydrodynamic and electroconducting flows. Ed. Aleman, Marty & Thibault. Kluwer, Dordrecht 1999.
- [10] Boissonneau P., Byrne P. An experimental investigation of hydrogen gas bubble-induced free convection in a small electrochemical cell.
- [11] Byrne P., Fontes E., Cournet N., Herlitz F., Lindbergh G. A simulation of the tertiary current density distribution from a chlorate cell. I: Mathematical model. *Accepted by J. Electrochem. Soc.* 2001.
 - A simulation of the tertiary current density distribution from a chlorate cell. II: Experimental study. Submitted to J. Electrochem. Soc. 2001.
- [12] Chapman B., Leighton D.T. Dynamic viscous resuspension. Int. J. Multiphase flow, (1991), 17:4, pp. 469-483.
- [13] Chisti M.Y. Airlift Bioreactors, 1989. Elsevier Science Publisher Ltd. ISBN 1-85166-320-7.
- [14]
- [15] Crowe C.T., Sommerfeld M., Tsuji Y. Multiphase flows with droplets and particles. CRC Press LLC 1998. ISBN 0-8493-9469-4
- [16] Dagan Z. Pfeffer R. and Weinbaum S., 1982. Axisymmetric stagnation flow of a spherical particle near a finite planar surface at zero Reynolds number, J. of Fluid Mech., 122. pp. 273-294.
- [17] Dahlkild A.A. The motion of Brownian particles and sediment on an inclined plate. J. Fluid Mech. 1997.337 pp 25-47.
- [18] Dahlkild A.A, 2001. Modelling the two-phase flow and current distribution along a vertical gas-evolving electrode. J. of Fluid Mech., 428, pp. 249-272.
- [19] Drew D.A, Lahey R.T. The virtual mass and lift force on a sphere in rotating and straining inviscid flow. Int. J. Multiphase Flow, 1987. 13 1 pp. 113-121.
- [20] Durst F. Fluid Mechanics developments and advancements in the 20th century. 10th international symposium on applications of laser techniques to fluid mechanics, Lisbon, July 10-13, 2000.
- [21] http://mech.postech.ac.kr/fluidmech/history
- [22] Ghirardini M., Donati G., Rivetti F. 1992. Gas lift reactors: hydrodynamics, mass transfer and scale up. Chemical engineering Science, 47:9-11, 2209-2214
- [23] Hetsroni G. Handbook of Multiphase Systems, McGraw Hill, 1981
- [24] Hetsroni G. Banerjee S. Hewitt G.F. Yadigaroglu G. Quarini G.I. Lance M. 1996 Short Courses. Multiphase Flow and Heat Transfer. ETH Zürich.

- [25] Hine F. Hydrodynamic studies of bubbles effects on the IR-drop in a vertical rectangular cell. J. Electrochem. Soc. 122, pp. 1185-1190.
- [26] Hine F. & Murakami K. Bubble effects on the solution IR drop in vertical electrolyzer under free and forced convection. J. Electrochem. Soc. 127, pp. 292-297.
- [27] Happel J., Brenner H. Low Reynolds number Hydrodynamics, Noordhoff Intl. Pub., Leiden 1973.
- [28] CFX manual
- [29] Ishii M. Thermo Fluid Dynamic Theory of Two-Phase Flow. Eyrolles, Paris. 1975.
- [30] Ishii M. and Zuber N. Drag coefficient and relative velocity in bubbly, droplet or particulate flows. AIChE J., 1979, 25 pp. 834-855.
- [31] Janssen L.J.J., Behaviour of and mass transfer at gas evolving electrodes. *Electrochemica Acta*, (1989), **34:2**, pp. 161-169.
- [32] Lance M., Bataille J., Turbulence in the liquid phase of a uniform bubbly air-water flow. J. Fluid Mech. 222, pp. 95-118.
- [33] Lance M., Lopez de Bertodano M., Phase distribution and wall effects in bubbly flows. 3rd Int. workshop on two-phase flows fundamentals, London, June 15-19, 1992.
- [34] Leighton D., Acrivos A. The shear-induced migration of particles in concentrated suspensions. J. Fluid Mech. 1987, 181 pp. 415-439.
- [35] Lessard R.R., Zieminski A.S. Ind. Eng. Chem. Fundam., 10, 1971, p. 260.
- [36] Lindert M., Kochbeck B., Prüss., Warnecke H-J., Hempel D.C. 1992. Scale-up of Airlift-loop Bioreactors based on Modelling the Oxygen Mass Transfer. Chemical engineering Science, 47:9-11, 2281-2286.
- [37] Marucci G., Nicodemo L., Chem. Eng. Sci. 22, 1967, p. 1257.
- [38] Mclaughlin J.B. Inertial migration of small sphere in linear shear flows. J. Fluid Mech.. 1991. **224**, 261, 1991.
- [39] Mei R. An approximate expression for the shear lift on a spherical particle at finte Reynolds number. *Intl. J. Multiphase Flow*, 18, 145, 1992.
- [40] Nationalencyklopedien, 1989, Bokförlaget Bra Böcker AB., Höganäs, Sweden. ISBN 91-7024-619-X.
- [41] Newman J.S. Electrochemical Systems, Second Ed., Prentice-Hall, Englewood Cliffs, NJ, 1991.
- [42] Nicolai H., Herzhaft B., HinchE.J., Oger L. Guazelli E. Particle velocity fluctuations and hydrodynamic self-diffusion of sedimenting non-Brownian spheres. *Phys. Fluids.* 1995, **7:1**, pp. 12-23.
- [43] Prince J.P., Blanch., AI Chem. Eng. J. 36, 1990, p. 1485.
- [44] Rivière N., Cartellier A. Wall shear stress and void fraction in Poiseuille bubbly flows. Part I& II. Eur. J. Mech. B/Fluids 1999, 18, pp. 823-846 and 847-867.
- [45] Rubinov S.I., Keller J.B. The transverse force on spinning sphere moving in a viscous fluid. J. Fluid Mech. 11, 447, 1961.
- [46] Sadatomi M., Sato Y. & Saruwatari S. 1982. Two-phase flow in vertical noncircular channels. Int. J. Multiphase flow. 8:6, 641-655.
- [47] Saffman P.G. The lift on a small sphere in a slow shear flow. J. Fluid Mech. 1965, 22:2 pp. 385-400.
 Corrigendum: J. Fluid Mech. 1968 31 pp. 624.
- [48] Schaffinger U. Laminar transport of solid particles suspended in liquids. The Flow of Particles in Suspensions (ed U. Schaffinger). Springer. 1996.
- [49] Schlichting H. Boundary Layer Theory. A McGraw-Hill Classic Textbook Reissue. 1987.
- [50] De La Rue R.E., Tobias C.W. J. Electrochem. Soc. 1959, 106, p. 827
- [51] Tobias C.W. *ibid*. 1959, **106**, p. 833
- [52] Meredith R.E., Tobias C.W. *ibid.* 1963, **110**, p. 1257
- [53] Wallgren C.F., Bark F.H. & Andersson B.J. Electrolysis of a binary electrolyte in twodimensional channel flow. *Electrochemica Acta*, (1996), 41:18, pp. 2909-2916.
- [54] G.B. Wallis. One-dimensional two-phase flow. 1969. McGraw-Hill.
- [55] Vogt H. 1983. Gas evolving electrodes. Comprehensive treatise of electrochemistry.6 445-489.
- [56] Walsh F. A first course in electrochemical engineering. 1993. The Electrochemical Consultancy, England. ISBN 09517307
- [57] Ziegler D., Evans J.W. Mathematical modelling of electrolyte circulation in cells with Planar Vertical Electrodes. J. Electrochem. Soc. 1986, 103:3, p. 567-576.
- [58] Zuber N., Finlay J.A. J. Heat Transfer 87, 1965, p.453